The P2X4 purinergic receptor controls the autophagy-related release of small extracellular vesicles from mammary cancer cells under hypoxia

Thomas Duret, Mohammed Elmallah, Audrey Heraud-Meley, Cloe Tessier, Ana Valeria Vinhais da Silva, Stéphanie Chadet, Roxane Lemoine, Justine Gainche, Valérie Labas, Ana-Paula Teixeira-Gomes, et al.

Cell Communication and Signaling

RESEARCH

Open Access

The P2X4 purinergic receptor controls the autophagy-related release of small extracellular vesicles from mammary cancer cells under hypoxia

Thomas Duret[1], Mohammed Elmallah[1], Audrey Heraud-Meley[1], Cloé Tessier[1], Ana Valeria Vinhais Da Silva[1], Stéphanie Chadet[1], Roxane Lemoine[2], Justine Gainche[1], Valérie Labas[3,4], Ana-Paula Teixeira-Gomes[3,4], Daniel Tomas[3,4], Vesna Cuplov[1], Lin-Hua Jiang[1,5,6], Lili Fan[1,7], Gang Yin[1,7], Christophe Baron[1,8,9] and Sébastien Roger[1,9*]

Abstract

Background Small extracellular vesicles (sEVs) are critical mediators of cell communications and are influenced by cellular stress. This study investigates the role of P2X4 and P2X7 purinoreceptors in the biogenesis and release of sEVs from triple-negative mammary cancer cells under hypoxia.

Methods In this study, we used CRISPR/Cas9 knockdown models from the triple-negative mammary cancer cell line 4T1 and selective pharmacology, to knock-down or inhibit either P2X4 or P2X7 receptors. We analysed intracellular endo-lysosomal compartments with transmission electron microscopy and epifluorecence imaging. The release and characterization of sEVs was analysed by nanoparticle tracking analysis, proteomics and western blotting. The incorporation of sEVs into recipient cells was followed by epifluorescent imaging and flow cytometry and consequences on cancer cell invasiveness was studied using transwell assays.

Results We found that P2X4 but not P2X7 regulates sEV release. P2X4 silencing increased the number of multivesicular bodies (MVBs), enhanced sEV production and selectively promoted CD9-positive sEV subpopulations under hypoxia. Proteomic analysis revealed altered sEV protein content in P2X4-deficient cells, including enrichment in epithelial markers and autophagic proteins (LC3-II, p62), and depletion of the endosomal sorting complexes required for transport (ESCRT) components required for endo-lysosomal fusion. This profile indicates a shift toward autophagy-dependent, unconventional sEV secretion via amphisomes. Additionally, sEVs from P2X4-deficient cells integrated more efficiently into recipient cancer cells but decreased their invasive capacity, suggesting functional consequences of altered sEV cargo. In contrast, intervention of P2X7 had no impact on sEV release.

Conclusions Overall, our findings identify the P2X4 receptor as a key regulator of hypoxia-induced sEV secretion and composition through modulation of endo-lysosomal trafficking and autophagy, with potential implication for tumour progression and intercellular signalling.

*Correspondence:
Sébastien Roger
sebastien.roger@univ-tours.fr

Full list of author information is available at the end of the article

Keywords P2X receptors, Extracellular vesicles, Secretive autophagy, Hypoxia, Cancer invasiveness

Introduction

Most cancer-related deaths result from the gain of aggressive traits and the development of metastasis originating from solid tumours. This is particularly true for epithelial cancers such as breast cancer, which remains the most lethal cancer among women worldwide [1]. Cancer progression towards metastatic stages relies on the selection of the cancer cells able to cope with the very stringent tumour microenvironment. Especially, they must adapt to metabolic challenges associated with the development of hypoxic cores and to nutrients deprivation in tumour regions distant from the vasculature. Consequently, surviving cancer cells exhibit various metabolic adaptations, such as increased glycolytic activity and macroautophagy (hereafter referred to as autophagy) [2], which enhance resistance to hypoxia and are generally associated with heightened tumour aggressiveness [3]. Additionally, tumour progression is driven by extensive local communications between tumour cells and their surrounding stromal and immune cells [4]. Moreover, tumour cells release soluble factors that induce phenotypic changes in distant tissues (e.g., bone), facilitating the formation of pre-metastatic niches [5]. Notably, cancer cells release extracellular vesicles (EVs), particularly small EVs (sEVs) under 200 nm in size, at significantly higher levels than normal cells. These sEVs contribute to tumour growth, development, and metastasis [6]. Hypoxic and metabolic stresses, both recognized as key drivers of tumour progression [7], have been shown to enhance the production and release of sEVs [8]. These vesicles act as potent messengers, circulating through extracellular spaces and bodily fluids to modulate the phenotype and function of recipient cells, whether nearby or at distant sites. EVs are heterogeneous in size, origin, and composition. Subtypes include small EVs (< 200 nm), such as exosomes (30–150 nm), as well as ectosomes/microvesicles (100–1,000 nm) and apoptotic bodies (100–5,000 nm). sEVs deliver a variety of cargos, proteins, lipids, and nucleic acids, to recipient cells. Their secretion is a complex, multistep process involving the endocytic pathway. sEVs are initially formed as intraluminal vesicles (ILVs) within multivesicular bodies (MVBs), through inward budding of the endosomal membrane. Fusion of MVBs with the plasma membrane then releases ILVs as sEVs [9]. These sEVs circulate in all body fluids and are responsible for either short- and long-distance communications. The fusion of MVBs to the plasma membrane requires the participation of the endosomal sorting complex required for transport (ESCRT) components [10] and associated proteins, such as nSmase2 [11] and the CD63 tetraspanin [12]. Alternatively, MVBs may also fuse with lysosomes, resulting in the degradation of their content [13]. This decision is orchestrated by specific Rab GTPases [14], from the Ras superfamily of small GTPases, as well as by SNARE proteins (soluble N-ethylmaleimide-sensitive factor attachment protein receptors) [15].

Autophagy is a crucial degradation and recycling mechanism that maintains cellular homeostasis and promotes survival under nutrient deprivation conditions. During autophagy, autophagosomes engulf cytoplasmic components and subsequently fuse with lysosomes to degrade their contents [2]. Increasing evidence suggests that sEV biogenesis and autophagy are interconnected processes that may share common regulatory mechanisms [16]. Metabolic stressors such as hypoxia can alter sEV biogenesis and secretion by promoting the formation of amphisomes, hybrid organelles resulting from the fusion of autophagosomes with MVBs. These amphisomes typically fuse with lysosomes, leading to the degradation of sEVs. However, when this fusion is impaired, a process known as "secretory autophagy" may occur. This mechanism allows for the extracellular release of sEVs enriched with autophagy markers such as SQSTM1/p62 and LC3-II [17–19]. Such changes in the EV proteomic contents can influence their biological activity and potentially contribute to increased cancer aggressiveness [20]. Despite the recognized importance of sEVs in cancer progression, the molecular determinants governing MVB formation, and the mechanisms directing their fusion either to the plasma membrane or to autophagosomes, remain largely unresolved.

The purinergic signalling is a powerful communication involved in both autocrine and paracrine cell communications, mainly mediated by extracellular adenosine 5'-triphosphate (ATP), but also by some other nucleotides such as adenosine 5'-diphosphate (ADP), uridine 5'-triphosphate (UTP), uridine 5'-diphosphate (UDP) or even UDP-glucose. These nucleotides are released into the extracellular space in response to diverse stimuli such as hypoxia and ischemia, mechanical stress or electrical stimulation [21]. Extracellular ATP, via activating membrane-spanning receptors of the P2 family [21], regulates key physiological functions and basal tissue homeostasis and, moreover, are participates in several diseases including inflammatory diseases and cancer [22–24]. P2 receptors are categorized into two distinctive subfamilies: ATP-gated ion channel P2X receptors, comprising of seven members P2 × 1-P2X7 [25], and G-protein-coupled P2Y receptors, accounting for eight members ($P2Y_1$, $P2Y_2$, $P2Y_4$, $P2Y_6$, $P2Y_{11}$-$P2Y_{14}$) in human [26]. This communication pathway is proposed to be restricted in space and time due to desensitization of receptors (with

the exception of P2X7 that does not desensitize [27]) combined with the prompt activity of ectonucleotidases hydrolysing extracellular nucleotides [28]. However, evidence suggests that purinergic receptors may also be involved in long distances cell-to-cell communications and within prolonged durations through the release of EVs [29].

P2X receptors function as ATP-gated, non-selective cation channels, permeating K^+, Na^+ and Ca^{2+}, thus mediating membrane depolarization and intracellular Ca^{2+} influx [30]. Several P2X receptors are strongly implicated in cancer growth and aggressiveness [31]. Among these, the P2X7 receptor has attracted particular attention for its role in tumour growth [32], supporting cancer cell invasiveness and metastatic progression [33–35] as well as in tumour-associated inflammation [36]. This receptor, key to initiating inflammatory responses via NLRP3 inflammasome activation and the release of IL-1β and IL-18 [37], has also been implicated in the release of microvesicles from immune cells [38–40] and pro-metastatic exosomes from melanoma cells [41]. Recently, P2X4 has also emerged as a significant player, overexpressed in cancers. Although primarily localized to endo-lysosomal compartments [42], it has been associated with invasion and metastasis in prostate [43, 44] and breast [45] cancers. Notably, we previously demonstrated a central role for P2X4 in mediating lysosome–autophagosome fusion and in sustaining autophagy in cancer cells [45]. In other models, such as HCV-infected hepatocytes, P2X4 has been linked to exosome release [46].

In this study, we aimed to elucidate the roles of P2X4 and P2X7 in sEV biogenesis and secretion by aggressive mammary cancer cells under hypoxic conditions, which are known to promote autophagy. We have identified a specific and essential role for P2X4, but not P2X7, in regulating the release of pro-invasive sEV populations via a secretory autophagy pathway.

Methods

Pharmacological ligands and inhibitors

The P2X4 antagonist 5-BDBD and the P2X7 antagonist A438079 were both purchased from Tocris (Bio-Techne, France). P2X agonists 2′(3′)-O-(4-benzoylbenzoyl) adenosine 5′-triphosphate (BzATP) and adenosine 5′-triphosphate (ATP), the autophagy inhibitor chloroquine and the n-SMase2 inhibitor GW4869 were purchased from Sigma-Aldrich (France). GW4869 was dissolve in DMSO as a suspension stock of 10 mM, then diluted to a working concentration of 10 µM in culture medium.

Cells and cell culture

The murine triple-negative (ER^-, PR^-, $HER2^-$) mammary cancer cell line 4T1 from the Balb/cJ strain was purchased from LGC Standards (France) and a stable 4T1-luc cell line expressing the luciferase gene was obtained by transduction of cells with lentiviral vectors containing the luciferase gene and blasticidin resistance gene for selection (GIGA Viral Vectors, Belgium) as already described [35, 45]. A stable cell line not expressing the P2rx4 gene, hereafter called "CR4", was obtained using the CRISPR/Cas9 technique by transfection with the P2rx4 Double Nickase Plasmid (Santa Cruz, France) as previously described [45]. Similarly, a stable cell line not expressing the P2rx7 gene, hereafter called "CR7", was obtained using the CRISPR/Cas9 technique by transfection with the P2rx7 Double Nickase Plasmid (Santa Cruz, France) [35]. Furthermore, a null-target Double Nickase Plasmid was also used to transfect 4T1-luc cells, leading to the generation of a control cell line, thereafter called "CTL" cell line. In all cases, clonal selections were performed by cell sorting using FACS melody (BD Biosciences, France). Efficiency of CRISPR-mediated knockdown was assessed by RT-qPCR and western blotting. Stability of clones was maintained for a minimal duration of 8 weeks after selection. All cell types generated from 4T1 cells were cultured in Roswell Park Memorial Institute 1640 medium (RPMI 1640, Gibco, France) supplemented with GlutaMAX (Gibco, France, ref. 61870036) and 10% foetal bovine serum (FBS, Hyclone, Cytiva SH30071.03). For normoxia experiments, cells were grown at 37 °C in a humidified 5% CO_2 incubator. For hypoxia experiments, cells were grown in a hypoxic chamber (Invivo 200, Ruskinn Technology, France) under the following conditions: 1% O_2, 5% CO_2 and 94% N_2.

RNA extraction, reverse transcription, and quantitative polymerase chain reaction (qPCR)

Total RNA was extracted using trizol/chloroform partitioning methods. Briefly, 1 mL of TRIzol was added to 10^5 cells for lysis and mixed with ½ volume of chloroform. After centrifugation, the upper phase was recovered and then mixed with 500 µL isopropanol. After centrifugation for 15 min at 12 000 x *g*, the pellet containing total RNA was washed twice with ethanol 75%, then dried and re-suspended in 15–25 µL ultrapure water. RNA yield and purity were determined by spectrophotometry using a NanoDrop™ One (Thermo Fisher Scientific; Waltham, MA) and only those samples with A260/A280 and A260/A230 ratios above 1.9 were kept for further experiments. Reverse transcription of 1 µg of total RNA was carried out using the PrimeScript™ RT reagent Kit (Takara, Shiga, Japan) in a final volume of 20 µL of according to manufacturer's specifications. The expression of genes of interest was assessed by quantitative PCR (qPCR) using validated primers (Table 1) and SYBR qPCR Premix Ex Taq (Takara, France). Cycling was carried out using a CFX CONNECT (Bio-rad, France) with the following conditions: a PCR activation step at 50°C

Table 1 Sequences of qPCR primers

Gene Name	Species	Forward primers 5′ → 3′	Reverse primers 5′ → 3′	Amplicon size (pb)
Rab27a	mouse	GGATAGAGCACAGCGAGGAC	TAGCGTCCTTAGCTGGAAGC	216
RalA	mouse	TGGCACATACTGACCAGACG	TCCTGGAATGCCTGAGTGTC	206
RalB	mouse	TGAACCATGACCACCACCAG	TCTGAGACTACAGGGGTGCA	176
Rab7	mouse	ACTTCGAGACCAGTGCCAAG	AAGGACTCTGTGCTCACTGC	197
Rab11	mouse	TGGAAGCCTGTCACTGTAGG	GCTGCTCTGTGGCAAAACAA	117
Rab35	mouse	AACAGCAGCAGCAACAACAG	GGGGAAAAGGGGAGGAAGTG	227
Rab8a	mouse	AAAACCGCCTCCCCAATCTT	GGCAGTCATTCTGGTTCCCA	159
Rab2b	mouse	TCCCCTCAGCAGAACGTTTC	TCGCACACTGAAAAGAGGCT	168
Eea1	mouse	CGCATACAGAGTCCCAGGTC	ACAACCCAGCACAACCTCAT	110
Lamp1	mouse	AGTGGCAACTTCAGCAAGGA	GGTCACCGTCTTGTTGTCCT	210
Lamp2	mouse	CTGCCACAACCAACTTCACC	GGCATCCCAGAAGCTAAGGT	203
Tbp	mouse	AAGG GAGAATCATGGACCAGAAC	GGTGTTCTGAATAGGCTGTG GAG	149
Gapdh	mouse	AATGGTGAAGGTCGGTGTG	GTGGAGTCATACTGGAACATGTAG	150
P2X4	mouse	CCTGGCTTACGTCATTGGGT	AAGTGTTGGTCACAGCCACA	113
P2X7	mouse	AGCACGAATTATGGCACCGT	CCCCACCCTCTGTGACATTCT	172

for 2 min followed by 95°C for 2 min, then 40 cycles of melting at 95°C for 15 s and annealing at 60°C for 30 s and extension at 72°C for 10 s. The gene encoding for TATA-binding Protein (TBP), was used as the reference gene. Levels of gene expression were normalized in each sample to the expression of internal reference gene and relativized to normal condition. Results are presented as fold change values calculated by the comparative $2^{-\Delta\Delta}$CT method as previously described [45].

Western blotting

Cells were washed twice with ice-cold PBS (Gibco, France) and then lysed with RIPA buffer including protease inhibitors (Roche Lifesciences, France). Protein concentration was measured using Pierce® BCA protein assay kits (Thermo Fisher Scientific, France) and 20 µg of total protein were resolved on 10% SDS-PAGE gels. After electrophoretic separation, proteins were transferred onto 0.2-µm nitrocellulose membrane (Thermo Fisher Scientific, France). Membranes were saturated for 1 h with 0.1% Tween Tris-buffered saline solution containing 5% bovine serum albumin (TBS-BSA) then incubated overnight with primary antibodies (Table 2). Membranes were washed 3 times in TBS-BSA during 10 min then incubated with corresponding secondary antibodies (Table 2) for 1 h at room temperature and washed 3 times for 10 min. Immunodetection of protein bands was revealed after 1 min incubation with the chemiluminescent substrate (SuperSignalTM West Pico PLUS Chemiluminescent substrate, ref34580, Thermo Fisher Scientific). Signals were acquired using the PXi imager (Labgene Scientific SA, Switzerland) and analysed with the Fiji software.

Isolation and characterization of small extracellular vesicles (sEVs)

For isolation of sEVs from CTL, CR4 or CR7, cells were cultured for 48 h at 80% confluence in RPMI 1640 supplemented with GlutaMAX medium and 10% EV-free FBS (HyClone, Cytiva SH30071.03) in either normoxic or hypoxic conditions. For isolation of sEV from CTL cells treated with either 5-BDBD (5µM) or A438079 (10µM), cells were grown for 24 h with RPMI1640 supplemented with GlutaMAX medium and 10% EV-free FBS, washed twice with PBS, and incubated 48 h with RPMI1640 supplemented with GlutaMAX and 10% EV-free FBS in presence of antagonists or vehicle. Supernatants of cells were collected and centrifuged at 480 x *g* during 5 min, and then at 2,000 x *g* for 15 min to remove cellular and non-cellular debris. Supernatants were further centrifuged at 10,000 x *g* during 45 min to remove large EVs. Supernatants were finally ultracentrifuged at 110,000 x *g* for 90 min. Pellets were washed with PBS and ultracentrifuged again at 110,000 x *g* for 90 min. Pellets, containing sEVs were resuspended in a final volume of 60 µL PBS without Ca^{2+} and Mg^{2+}. All relevant data from our experiments have been submitted to the EV-TRACK knowledgebase [47] and are accessible via the following URL: https://evtrack.org/review.php with EV-TRACK ID (EV230006).

Sizes and concentrations of sEVs were estimated from samples by nanoparticle tracking analysis (NTA, Zetaview PMX-120, Particle Metrix, Germany). Samples of purified sEVs were diluted in PBS (1:1,000–1:4,000) and injected in the sample chamber with sterile syringes. The proportion of CD9-, CD63- and CD81-positive subpopulations of EVs were estimated from same samples by Fluo-NTA (Zetaview PMX-120, Particle Metrix). Briefly, primary antibodies coupled with phycoerythrine (PE) were incubated for 2 h at room temperature: mouse

Table 2 Primary and secondary antibodies used for western blotting (WB) and immunocytofluorescence (IF) experiments

Antibodies directed against	References (companies)	Experiment type	Dilution
CD9	sc-13,118 (Santa Cruz Biotechnology)	WB	1/1000
CD63	sc-5275 (Santa Cruz Biotechnology)	WB	1/1000
CD63-APC	130-123-276 (Miltenyi Biotec)	IF	1/100
CD81	sc-166,029 (Santa Cruz Biotechnology)	WB	1/1000
Alix	2171 S (Cell signaling)	WB	1/1000
Tsg101	sc-7964 (Santa Cruz Biotechnology)	WB	1/1000
Flotilin-1	3253 S (Abcam)	WB	1/1000
Grp94	2104T (Cell signaling)	WB	1/1000
Eea1	ab2900 (Abcam)	WB	1/1000
Rab5	ab18211 (Abcam)	WB	1/1000
Rab7	ab137029 (Abcam)	WB	1/1000
Rab7	9367T (Cell signaling)	IF	1/200
Rab11	5589 S (Cell signaling)	WB	1/1000
Rab27a	CAB1934 (Assay genie)	WB	1/2000
Rab27b	CAB10389 (Assay genie)	WB	1/2000
Ral A	CAB11736 (Assay genie)	WB	1/2000
Ral B	CAB4069 (Assay genie)	WB	1/2000
β-actin	sc-47,778 (Santa Cruz Biotechnology)	WB	1/1000
HSC70	sc-7298 (Santa Cruz Biotechnology)	WB	1/1000
mouse IgG-HRP	Cat. 1,706,516 (Biorad)	WB	1/10,000
rabbit IgG HRP	Cat. 1,706,515 (Biorad)	WB	1/5000
rabbit IgG Alexa Fluor ^{TM} – 555	A31572 (Invitrogen)	IF	1/10,000

anti-CD9 (1: 6, ref. 130-123-052 Miltenyi Biotec, France), mouse anti-CD63 (1: 10, ref. 130-108-923 Miltenyi Biotec, France) and mouse anti-CD81 (1: 10, ref. 130-102-632 Miltenyi Biotec, France). Samples were diluted in PBS (1:1,000–1:2,000) and injected in the sample chamber with sterile syringes. Measurements were performed at 25 °C on 11 positions, using EV480nm.

Fluorescent staining and uptake of sEVs

Isolated small EVs were labelled using the green, fluorescent membrane dye PKH67 using Fluorescent Cell Linker kits (PKH67GL, Sigma-Aldrich). EV pellets were resuspended with 500 µL of Diluent C and mixed with 4 µL of PKH67 pre-diluted with 500 µL of Diluent C for 5 min at room temperature. Reaction was stopped with 4 mL of PBS-10% BSA during 1 min. Samples were completed to 40 mL with medium without serum and EVs were ultracentrifuged at 110,000 x *g* for 90 min to remove dye in excess. EVs pellets were washed twice with PBS by ultracentrifugation using the same conditions.

Immunocytofluorescence

Cells (5×10^4) were seeded on 18-mm sterile coverslips and cultivated in 24-well plates under hypoxia for 24 h. Cells were then washed with PBS kept in 1% O_2 and fixed with 4% paraformaldehyde for 15 min at room temperature. After two washes with PBS containing Ca^{2+} and Mg^{2+}, cells were permeabilized with 0.1% Triton X-100 and 0.2% BSA for 15 min, then washed twice. Saturation of epitopes was realized with 3% BSA in PBS during 20 min at room temperature. Cells were incubated overnight at 4°C with anti-Rab 7 antibody (Cell Signaling Technology, USA, 9373T) diluted in 1% BSA prepared in PBS. Cells were then washed three times with PBS containing Ca^{2+} and Mg^{2+} for 10 min, then incubated for 1 h with the corresponding secondary antibody coupled with fluorochrome in 1% BSA. For CD63 staining, we used a flow cytometry antibody conjugated with allophycocyanin (APC, Miltenyi Biotec, France, 130-123-276), for 2 h at room temperature in the dark. Cells were then washed three times with PBS containing Ca^{2+} and Mg^{2+} for 10 min. Coverslip were washed three times with PBS containing Ca^{2+} and Mg^{2+} for 10 min, then mounted on slides using ProLong Gold antifade reagent containing DAPI for visualization of nuclei.

Flow cytometry

Prior to conducting experiments, cells were seeded at a density of 10^5 per well of 6-well plates. They were cultured in either normoxia or hypoxia, as previously described, for a duration of 24 h. Cells were treated with ATP (at concentrations indicated in figure legends) or BzATP (300 µM) for 2 h and then washed with PBS. Cells were detached using trypsin-EDTA and centrifuged 5 min at 480 x *g*. Supernatants were discarded, and cells were further washed with PBS. Cells were fixed and permeabilized with BD CytoFix/CytoPerm ^{TM} (BD Biosciences, France) 20 min at 4 °C, then washed with BD

Perm/Wash™ (BD Biosciences, France). Cells were stained with anti-CD9-PE, anti-CD63-PE and anti-CD81-PE antibodies, washed and re-suspended with PBS containing 1% BSA containing 0.01% sodium azide. Fluorescence data were acquired using a BD Melody FACS cytometer (Becton Dickinson, France) and analysed with FlowJo software.

Cell viability

The assessment of cell viability was performed using the 3-[4,5-dimethylthiazol-2-yl]-2,5 diphenyl tetrazolium bromide (MTT) assay as previously described [34]. Briefly, cells were cultured for 5 days then incubated with 0.5 mg/mL MTT at 37 °C for 1h. To test the effect of isolated sEVs on cell viability, cells were grown in 48-well plates and were treated with purified sEVs (5×10^3 sEVs per cell), every day for 3 days. Cells were incubated for 1 h with 0.5 mg/mL MTT. Resulting formazan crystals were dissolved in DMSO and the absorbance was measured at 560 nm using a plate reader (Varioskan Lux, Thermo Fisher Scientific, France).

Co-culture and invasion assays

For co-culture assay, 5×10^4 CTL, CR4 or CR7 cancer cells were seeded at the bottom of 24-well plates and grown for 24 h under either normoxic or hypoxic conditions in 800 µL OptiMEM medium containing no FBS. Inserts containing an 8-µm pore-sized polyethylene terephthalate filter membrane pre-coated with Matrigel® matrix (Corning, France) were placed in each well. Then, 6×10^4 CTL cells, formerly cultivated under normoxia or hypoxia were seeded in upper chamber of the invasion inserts in 200 µL of OptiMEM medium containing no FBS. After 24 h of invasion, inserts were washed twice in PBS containing Ca^{2+} and Mg^{2+}, and cells were fixed for 10 min in cold methanol. Inserts were further washed twice in PBS and cells that had invaded and adhered to the lower surface of the insert were stained with DAPI. Nuclei were imaged using the 10x objective on an EVOS M7000 microscope (Thermo Fisher, France), then counted and analysed using ImageJ software.

Cellular electrophysiology

Electrophysiological recordings of ATP-induced ion currents were performed in the whole-cell configuration of the patch clamp technique. Patch pipettes were pulled from borosilicate glass (World Precision Instruments, France) to a resistance of 4–6 MΩ. Currents were recorded using an Axopatch 200B amplifier (Axon Instrument, USA) and analogical signals were filtered at 10 kHz and digitized using a 1322A Digidata converter. Cell capacitance and series resistance were electronically compensated. Membrane potential was clamped at -60 mV. Experiments were performed at room temperature in extracellular physiological saline solution containing (in mM): 147 NaCl, 10 N-2-hydroxyethylpiperazine-N'-2ethansulphonic acid (HEPES), 13 D-glucose, 2 KCl, 2 $CaCl_2$ and 1 $MgCl_2$. pH was adjusted to 7.4. Glass pipettes were filled with intracellular saline solution (in mM): 147 NaCl, 2 KCl ,10 HEPES and 10 ethylene glycol-bis-(2-aminoethyl ether)-N, N, N', N'-tetraacetic acid (EGTA). pH was adjusted to 7.3. ATP was externally applied using a RSC160 fast-flow delivery system (Bio-Logic Science Instruments, France) for a duration of 10 s, at a concentration of 3 mM.

Epifluorescence imaging

For epifluorescence microscopy experiments, cells were grown for 24 h on 18 mm coverslips in 21% or 1% O_2. Cells were fixed in 4% paraformaldehyde and then permeabilized with 0.1% Triton-X-100 for 15 min. Unspecific antibody binding was blocked with 3% BSA for 20 min. Primary antibody for P2X4 (Alomone, APR-002, 1:200) was incubated for 2 h at room temperature. Cells were then washed three times with PBS and incubated with diluted Alexa Fluor 647-conjugated secondary antibodies for 1 h. Plasma membrane was stained with Wheat Germ Agglutinin (WGA) conjugated to Alexa Fluor 488 (W11261, Thermofisher Scientific, France). Coverslips were mounted on slides using ProLong® Gold Antifade Mountant containig DAPI for nuclei visualization (Invitrogen, France). Images were obtained using epifluorescence microscope (EVOS M7000, 40x objective, Thermofisher scientific, France) and were analysed using ImageJ software.

Transmission electron microscopy (TEM)

Cells were grown for 24 h in either 21% or 1% O_2 and then fixed for 24 h in a solution of 4% paraformaldehyde and 1% glutaraldehyde (Sigma, St-Louis, MO) in 0.1 M phosphate buffer (pH 7.2). Samples were washed in PBS and post-fixed by incubation with 2% osmium tetroxide (Agar Scientific, Stansted, UK) for 1 h. Cells were then fully dehydrated in a graded series of ethanol solutions and propylene oxide. The impregnation step was performed with a mixture of (1 : 1) propylene oxide and epon resin (Sigma Aldrich, France) and then left overnight in pure resin. Samples were then embedded in epon resin (Sigma Aldrich, France), which was polymerized for 48 h at 60 °C. Ultra-thin Sect. (90 nm) of these blocks were obtained using a Leica EM UC7 ultramicrotome (Leica Miscrosystems, Germany). Sections were stained with 2% uranyl acetate (Agar Scientific, UK), followed by 5% lead citrate (Sigma Aldrich, France).

For analyses of purified sEVs, 10 µL of sample coming from ultracentrifugation-based isolation procedure were mixed with 10 µL of TRUMP buffer (4% paraformaldehyde, 1% glutaraldehyde, 0.1 M phosphate buffer) and

conserved at 4 °C for fixation. Samples were incubated 2 min on grids, washed 3 times with purified distilled water (Versylène, Fresenius) and incubated for 1 min with a contrast solution (uranyl acetate 2%). Samples were observed using a JEOL 1400 plus transmission electron microscope (120 kV, JEOL, Tokyo, Japan), from the microscopy department of Inserm US61, University of Tours, France.

Proteomic analyses

Small EVs isolated and purified as previously described and stored at -80 °C were thawed on ice. For total protein extraction, sEV samples were homogenized in 50 µL of lysis buffer (50 mM Tris-HCl, pH 7.4, 2% SDS, 1/20 proteases inhibitors (P2714; Sigma Aldrich, France) for 30 min with thermomixer at 4 °C for 1,000 rpm. Samples were homogenized using a Bioblock sonicator five times, each for 20 s. After homogenization, samples were centrifuged at 10,000 x *g* for 30 min at 4 °C and supernatants were stored at – 20 °C. Protein concentration was determined using the Uptima BC Assay Protein Quantitation kit (Interchim, France) according to the manufacturer's instructions and using BSA as the standard. Efficiency of protein extraction was verified by SDS-PAGE. For that, samples were mixed with 2x sample buffer (125 mM Tris HCl pH 6.8, 4% SDS, 20% glycerol, 10% TCEP and 0.004% bromophenol blue), heated at 95 °C for 5 min and briefly centrifuged. Samples (15 µg) and the Bio-Rad protein markers Precision Plus Protein™ Dual Color Standards (2 µL) were loaded on to a 4–20% precast polyacrylamide gel (Mini-PROTEAN TGX Precast Protein Gels, Bio-Rad, France) and electrophorized at 200 V for 45 min (Mini-PROTEAN 3 electrophoresis cell, BioRad, France). The gel was then stained overnight with 5% Coomassie Blue R-350 (PlusOne™ Coomassie™ Blue PhastGel™ Blue R, GE Healthcare, France) in 30% ethanol/10% acetic acid. After staining, the gel was washed with Milli-Q water and 30% ethanol/10% acetic acid to remove background Coomassie stain and kept in 2% v/v acetic acid. The protein extracts were pooled by condition. 100 µg of total protein from each pool (2 × 50 µg) were fractionated on a 4–20% precast polyacrylamide gel at 150 V for 120 min. Precision Plus Protein Dual Color standards (Bio-Rad, France) were used as molecular weight standards (MW). After staining with Coomassie Blue R-350 (PhastGel Blue R, GE Healthcare), each gel lane was cut into 20 gel bands and subjected to in-gel digestion.

Gel pieces were washed in water: acetonitrile solution (1:1, 5 min) followed by 100% acetonitrile (10 min). Reduction and cysteine alkylation were performed by successive incubation with 10 mM dithiothreitol (DTT) in 50 mM NH_4HCO_3 (30 min, 56 °C), then 55 mM iodoacetamide in 50 mM NH_4HCO_3 (20 min, at room temperature in the dark). Pieces were then incubated in a 1:1 mixture of 50 mM NH_4HCO_3 and acetonitrile (10 min) followed by an incubation in acetonitrile (15 min). Proteolytic digestion was carried out overnight using 25 mM NH_4HCO_3 with 12.5 ng/µL trypsin (Sequencing grade, Roche diagnostics, France). Resulting peptides were extracted by incubation in 5% formic acid (sonicated) with the supernatant removed and saved, followed by incubation in water: acetonitrile and 1% formic acid (1:1, 10 min) and a final incubation with acetonitrile (5 min), again supernatant was removed and saved. These two peptide extractions were pooled and dried using a SPD1010 speedvac system (ThermoSavant, Thermo Fisher Scientific, Germany). The resultant peptide mixture was desalted and enriched with SPIN Columns C18 (Millipore, France) and dried again before being analyzed by nanoflow liquid chromatography tandem mass spectrometry (NanoLC-MS/MS). All nanoLC-MS/MS analyses were performed, in technical triplicate, at the PIXANIM platform (INRAE, Nouzilly, France) on a dual linear ion trap Fourier Transform Mass Spectrometer (FT-MS) LTQ Orbitrap Velos Pro (Thermo Fisher Scientific, Germany) coupled to an Ultimate® 3000 RSLC Ultra High-Pressure Liquid Chromatographer (Thermo Fisher Scientific, Germany) controlled by Chromeleon Software (version 6.80 SR13). Samples were desalted and concentrated for 10 min at 5 µL/min on a trap column (Acclaim PepMap 100 C18, 75 µm inner diameter x 2 cm long, 3 µm particles, 100 Å pores). The peptide separation was conducted using a nano-column (Acclaim PepMap C18, 75 µm inner diameter x 50 cm long, 2 µm particles, 100 Å pores) at 300 nL/min by applying gradient consisted of 2–45% B during 90 min. Mobile phases consisted of (A) 0.1% formic acid, 97.9% water, 2% acetonitrile (v/v/v) and (B) 0.1% formic acid, 19.9% water, and 80% acetonitrile (v/v/v).

Data were acquired using Xcalibur version 3.0.63 software (Thermo Fisher Scientific, San Jose, CA), in positive data-dependent mode in the 300–1800 m/z mass range. Resolution in the Orbitrap was set at $R = 60{,}000$. The 20 most intense peptide ions with charge states ≥ 2 were sequentially isolated (isolation width 2 m/z, 1 microscan) and fragmented in the high-pressure linear ion trap using CID (collision induced dissociation) mode (collision energy 35%, activation time 10 ms, Qz 0.25). Dynamic exclusion was activated during 30 s with a repeat count of 1. The lock mass was enabled for accurate mass measurements. Polydimethylcyclosiloxane (m/z, 445.1200025, $(Si(CH_3)_2O)_6$) ion was used for internal recalibration of the mass spectra MS/MS. Ion searches were performed using Mascot search engine version 2.7.0.1 (Matrix Science, UK) via Proteome Discoverer 2.5 software (Thermo Fisher Scientific, Germany) against the *Mus musculus* NCBI protein database (2023/07). The search parameters included trypsin as a protease with two allowed missed

cleavages and carbamidomethylcysteine, methionine oxidation and acetylation of N-term protein as variable modifications. The tolerance of the ions was set to 5 ppm for parent and 0.8 Da for-fragment ion matches. Mascot results obtained from the target and decoy databases searches were subjected to Scaffold Q + S v5.2.2 and Scaffold Quant v5.0.3 softwares (Proteome Software, Portland, USA) using the protein cluster analysis option (assemblage of proteins into clusters based on shared peptide evidence). Peptide and protein identifications were validated using the Peptide Prophet and Protein Prophet algorithms with a probability of 95% for proteins and 99% for peptides generating a FDR < 0.25% on proteins and FDR < 0.011% on peptides. Protein identifications were accepted if they contained at least two identified peptides. The data were normalized and quantified using the eXtracted Ion Chromatogram (XIC) approach in Scaffold Quant. The normalized average Precursor Intensity values were transformed using the logarithm (Log_{10}) and statistical analysis as t-test was performed. A Fold Change (FC) was also calculated (Log_2 Fold Change of Precursor Intensity) between the two conditions to determine the relative abundance level of each protein. The protein list was filtered based on the following criteria: $p \leq 0.05$ and a fold change of 2 ($Log_2(FC) \geq 1$ or $\leq$ -1) to identify differentially abundant proteins (DAP).

Data were processed with BioDBnet db2db (https://biodbnet-abcc.ncifcrf.gov/db/db2db.php) to get Gene ID and Gene symbol. Human orthologs gene has been obtained by BioDBnet dbOrtho (https://biodbnet-abcc.ncifcrf.gov/db/dbOrtho.php). Data has been organized by FunRich 3.1.3 software [48] and compared with VesiclePedia databank [49]. Cellular component and Biological process analysis were performed with FunRich 3.1.3 software using Gene ontology database.

List of genes implicated in late endosome/MVBs transport and fusion to lysosome, early endosome transport, endosome maturation, autophagy and exosome assembly were selected with the following methods: Biological process analysis of Differential (1.5 fold change) EVs from CTL and CR4 genes list has been performed using Gene ontology database on PANTHER website (https://geneontology.org/). Significant GO terms including key word « exosome, endosome, multivesicular bodies, endosome, lysosome or autophagy » have been reported. Genes from our differential list reported in these GO terms have been extracted. Z-scores of these genes have been calculated using precursor intensity and represented with heat map and dendrogram clustering using Heatmapper2/Expression module (https://heatmapper2.ca/site/expression/index.htm). Interaction analyses were performed with STRING: functional protein association network v12 (https://string-db.org/) website (minimum interaction score of 0.7). Results of proteomic analyses are provided in the Supplementary Table 1.

Statistical analyses

Graphs and statistics were performed using GraphPad Prism v.9.0.0 Software. Data were displayed as mean ± s.e.m. (standard error of the mean) or as median ± interquartile range as indicated in the figure legends, depending on the distribution of sample whether they follow a Gaussian distribution or not, respectively. For box plots, the upper and lower edges of the box indicate the first and third quartiles (25th and 75th percentiles) of the data and the middle line indicates the median. Mann-Whitney rank sum test, Wilcoxon matched-pairs signed rank test and two-tailed Student's t-tests were used for comparisons between two groups. Kruskal-Wallis, one- or two-way ANOVAs were used for comparisons of more than two groups. The size of samples (number of experiments, n) is indicated in the figure legends. Significant results are represented using p-value: *, $p < 0.05$; **, $p < 0.01$; and ***, $p < 0.001$. NS stands for no significance.

Results

Mammary cancer cells produce and release sEVs in both normoxic and hypoxic conditions

Previous studies have shown that in the aggressive triple-negative murine mammary 4T1 cancer cell line, the P2X7 receptor was mainly expressed at the plasma membrane of cells, responsible for ATP- or BzATP-induced inward currents. In these cells, only the P2X7 and no other P2X receptor was functional at the plasma membrane [35]. Differently, the P2X4 receptor has been demonstrated to be mainly expressed in acidic intracellular compartments [45] (Suppl. Figure 1a). To assess the impact of P2X4 and P2X7 expression on sEVs, we used stable clones with reduced expression of either P2X4 (CR4) or P2X7 (CR7) from the 4T1 cancer cell line, compared to a null-target CRISPRCas9 cell line (CTL), as previously described [35, 45]. The efficiency of P2rx4 and P2rx7 knock-downs was reassessed by RT-qPCR in comparison to CTL cells, under normoxic conditions (21% O_2). The results showed strong inhibition of P2rx4 in CR4 cells (> 76%) and of P2rx7 in CR7 cells (> 90%). Furthermore, P2rx7 expression was unchanged in CR4 cells, but a significant decrease of P2rx4 expression was significantly decreased by approximately 50% in CR7 cells (Suppl. Figure 1b).

Knocking-down the expression of P2rx7 gene was responsible for the disappearance of ATP-induced inward currents (Suppl. Figure 1c).

The presence of MVBs was assessed by transmission electron microscopy in all cell lines under both normoxic and hypoxic conditions (1% O_2) (Fig. 1a-b). Since the discrimination of endosomal-related structures containing

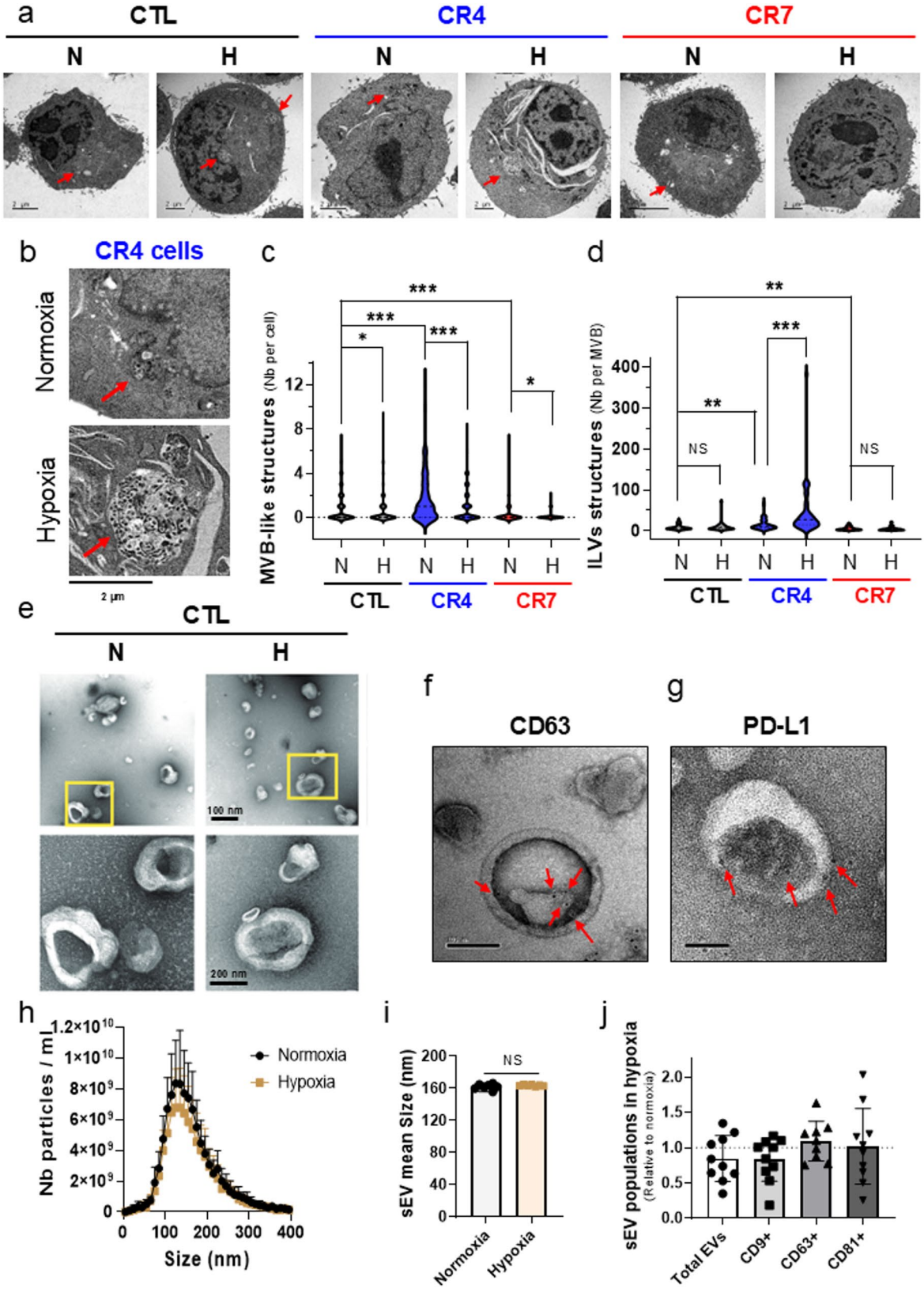

Fig. 1 (See legend on next page.)

(See figure on previous page.)

Fig. 1 Analyses of intracellular MVB-like structures and nanometer-sized sEV production by 4T1 mammary cancer cells under normoxic and hypoxic conditions. **a** Representative transmission electron micrographs illustrate formation of MVB-like structures (red arrows) in CTL, CR4 and CR7 cells, grown either under normoxic (N, 21% O2) or hypoxic (H, 1% O2) conditions for 24 h. Scale bar, 2 µm. **b** Representative example of MVB-like structures identified in CR4 cells (red arrows) grown under normoxia or hypoxia, demonstrating the presence of Intra-Luminal Vesicles (ILV). Scale bar, 2 µm. **c** Quantification of MVB-like structures per cell in same conditions than a expressed in violin plot. n = 177 to 202 cells, from 3 independent experiments. *, p<0.05; ***, p<0.001, Student's t-test. **d** Quantification of ILV per MVB-like structures in similar conditions than in a-b, expressed in violin blot. n = 45 compartments, from 3 independent experiments. N.S., stands for not statistically different; **, $p<0.01$; ***, $p<0.001$, Student's t-test. **e** Representative transmission electron micrographs of sEVs isolated from supernatants of CTL cells, grown either under normoxic (N) or hypoxic (H) conditions for 24 h. Scale bars, 100 and 200 nm. **f** and **g** TEM-immunogold labelling of native EVs isolated from supernatants of CTL cells grown in hypoxia. Pellets processed for immunogold labelling without permeabilization. **f** Using mouse monoclonal anti-human tetraspanin CD63 antibody and rabbit anti-mouse IgG conjugated to 10-nm gold particles (red arrows). Scale bar, 100 nm. **g** Using mouse monoclonal anti-human PD-L1 antibody and rabbit anti-mouse IgG conjugated to 10-nm gold particles (red arrows). Scale bar, 50 nm. **h** Size and quantity distribution of purified sEVs from CTL cells grown either under normoxia or hypoxia, assessed by NTA (n = 9 independent experiments in each condition). **i** Median size of purified sEVs, assessed as in h by NTA under both normoxia and hypoxia. N.S. stands for not statistically different. **j** Total number of sEVs and proportions of CD9+, CD63+ and CD81+ sEVs, assessed by Fluo-NTA, from supernatants of CTL cells cultivated under hypoxia, expressed relatively to normoxia (n = 10 independent experiments). There was no statistical difference

intraluminal vesicles (ILVs), such as MVBs and amphisomes, is difficult and tedious without specific labelling, we used the generic term of MVBs-like structures. These structures were identified in all three cell lines in both normoxia and hypoxia (Fig. 1a), and these were undoubtedly containing ILVs (Fig. 1b). Under normoxia, CR4 cells exhibited a drastic increase in the number of MVBs-like structures compared to CTL. This increase was also observed in CR7 cells but to a lesser extent (Fig. 1c). Under hypoxia, the number of MVBs-like structures per cell in CTL cells was mildly but significantly increased compared to that in CTL cells under normoxia. In contrast, the presence of these structures was significantly reduced in both CR4 and CR7 cells under hypoxia (Fig. 1c). Interestingly, the number of ILVs per MVB-like structures was significantly higher in CR4 cells compared to CTL and CR7 cells under normoxia, and further increased under hypoxia. In contrast, this parameter remained unchanged in either CTL or CR7 cells (Fig. 1d). These initial results suggested of a dysregulation in sEVs biogenesis in CR4 cells, which exhibited a specific decrease of P2rx4 expression.

These results prompted us to purify and analyse sEV, initially from CTL cells cultivated in normoxia or hypoxia. This was performed by differential ultracentrifugation (dUC), and scanning electron microscopy confirmed the release of particles showing a vesicular morphology in both conditions (Fig. 1e). Immunogold staining demonstrated that these particles expressed the CD63 tetraspanin (Fig. 1f) and the immune checkpoint inhibitor PD-L1 (Fig. 1g), both of which being conventional markers of cancer cells-derived sEVs [50, 51]. Analysis of the particle sizes indicated a majority of sEVs between 100 and 200 nm in diameter, consistent with exosome size, under both normoxia and hypoxia (Fig. 1h). There was no difference in the mean size of sEVs produced under normoxic or hypoxic conditions (161.9 ± 13 nm and 163.6 ± 41 nm, respectively, Fig. 1j). Furthermore, hypoxia did not increase the number of sEV being released (Fig. 1h) under our experimental conditions. We further analysed the proportion of $CD9^+$, $CD63^+$ or $CD81^+$ within the total sEVs population but did not identify any statistically significant changes under hypoxia. Only a non-significant tendency for a decrease in total and $CD9^+$ sEVs in hypoxia was observed compared to normoxia (Fig. 1j).

Inhibition of P2X4 increases the release of a specific $CD9^+$ subpopulation of sEVs under hypoxia

Because hypoxia is frequently encountered in solid tumours and is associated with an increased tumour aggressiveness, the following experiments were carried out under hypoxia (1% O_2), unless otherwise stated. sEVs were purified from CTL, CR4 and CR7 cells as described above. Analysis of particles size dispersion demonstrated a similar profile of sEVs coming from three cell types, with the majority of vesicles within 100–200 nm range size (Fig. 2a). Interestingly, knocking down the expression of P2X4 induced a significant increase in the median number of sEVs released by 32.7% compared to CTL under hypoxia (this was also observed under normoxia, Suppl. Figure 2a). In contrast, knocking down the expression of P2X7 had no significant effect (Fig. 2b) under hypoxia (and not under normoxia, Suppl. Figure 2a). Correspondingly, the loss of P2X4 was associated with an increase of protein concentration assessed from sEV extracts as compared to CTL. Again, the loss of P2X7 had no effect on protein concentration as compared to CTL but was significantly smaller than CR4 (Fig. 2c). The analysis of the quantity of sEVs released was obtained with genetically modified cells results. To rule out any selection bias, we performed similar analyses where CTL cells were treated with the P2X4 antagonist 5-BDBD (5 µM) or the P2X7 antagonist A438079 (10 µM). Similarly to the knock-down of the P2X4 receptor, its pharmacological antagonism also induced an increase in sEVs release under hypoxia. Antagonism of P2X7 induced no significant change in sEV release compared to the control condition (Fig. 2d). Median size of sEV produced by CR4 cells was significantly smaller than that of CTL cells (166.3 nm

and 175.6 nm, respectively). By contrast, knock-down of P2X7 induced no change in the median size of EVs compared to CTL (Fig. 2e, Suppl. Figure 2b). We also measured values of Zeta potential, correlated to the surface charge of vesicles, but noticed no change (average of -35 mV) between purified sEVs from CTL, CR4 or CR7 cells (Fig. 2f). We then quantified the proportion of $CD9^+$, $CD63^+$ and $CD81^+$ sEVs within the total number of sEVs. Interestingly, both P2X4 silencing (CR4) and antagonism (using 5-BDBD, 5 µM) selectively increased the release of $CD9^+$ sEVs (by 55.3 ± 28.4% and 42.2 ± 15.1%, respectively) with no change observed in the $CD63^+$ or $CD81^+$ subpopulations (Fig. 2g and h). By comparison, both P2X7 silencing (CR7) and antagonism (using A438079, 10 µM) had no effect on the differential release of $CD9^+$, $CD63^+$ and $CD81^+$ sEV subpopulations (Fig. 2i and j). We performed similar experiments on CTL cells under normoxia, assessing the concentrations of total sEVs and the proportions of $CD9^+$, $CD63^+$ and $CD81^+$ sEVs, when antagonizing specifically P2X4 or P2X7, but identified no difference (Suppl. Figure 1d-f), suggesting that this regulation only under a metabolic stress condition. We analysed intracellular levels of CD9, CD63, CD81 proteins by flow cytometry in CR4 and CR7 cells, compared to CTL. CD9 expression was significantly increased in CR4 cells, while CD63 and CD81 levels remained unchanged. In contrast, in CR7 cells, we measured the increase in all CD9, CD63, CD81 expression levels compared to CTL (Fig. 2k). The presence of marker proteins of sEVs was performed by western blotting from sEVs purified from supernatants, as well as from total cellular extracts for these three cell types (CTL, CR4 and CR7) cultured either under normoxia or hypoxia (Fig. 2l). In total cell extracts, there was no striking difference among all three cell types. As expected, we did observe no difference in the high levels of cytosolic markers HSC70 and β-actin, reticulum endoplasmic protein Grp94, CD63 marker of MVBs and ILVs, and detected at lower levels markers of CD9, CD81, Flotillin-1 and TSG101 used as ILVs markers. In the sEVs protein extracts, there was no immunodetection of Grp94, confirming the selectivity of our purification method, while we could identify specific markers of exosomes. Interestingly, in sEVs coming from CR4 cells, under both normoxia and hypoxia, we identified a higher level of CD9 in CR4 cells compared to CTL and CR7 cells, thus confirming previous results. At this stage, it is important to highlight that all experiments were performed in the absence of extracellular ligands of P2X receptors. Therefore, we also assessed the effect of stimulating CTL, CR4 or CR7 cells for 48 h under hypoxia, with extracellular ATP at concentration susceptible to activate P2X4 (30 and 100 µM) or with BzATP (300 µM) susceptible to also activate P2X7. However, we measured no quantitative change in the intracellular detection of tetraspanins CD9, CD63 and CD81 (Suppl. Figure 2c and d), and no effect on the concentration of sEVs or the $CD9^+$, $CD63^+$ and $CD81^+$ subpopulations (Suppl. Figure 2e-f). Taken together, these results identified a prominent role of P2X4 in the control of the release of $CD9^+$ sEVs under hypoxia, in the absence of exogenous stimulation. One could speculate that inhibition of P2X4 might lead to the intracellular accumulation of $CD9^+$ ILV and a correlative increase in $CD9^+$ sEVs. By contrast, inhibition of P2X7 induces no change in the secretion of total or subpopulation of sEVs.

P2X4 knockdown is associated with Rab7 increase and affects endo-lysosomal trafficking

We then further analysed the role of P2X4 in controlling the transport of endo-lysosomal compartments, which are involved in ILVs biogenesis and the fusion of MVBs to the plasma membrane and thereby release of sEVs. Notably, specific Rab GTPases are key regulators of these functions : Rab5 is involved in early endosome transport [52], Rab27a/b, RalA/B, Rab11 and Rab35 are controlling the transport of MVBs to the plasma membrane [14, 53], while Rab7 may participate in transport and fusion of MVBs to both lysosomes and plasma membrane [54, 55]. We also assessed the expression of EEA1 (early endosomal antigen 1), an effector of Rab5 involved in endosomal trafficking, as well as Lamp-1 and Lamp-2 that are expressed at the lysosomal membrane. First, qPCR experiment revealed that CR4 cells, not expressing P2X4, had a significant increase in the mRNA expression of RalA, RalB, Rab11, Rab35, Rab7, Lamp-1 and EEA1 compared to CTL, while CR7 cell only demonstrated an increase in Lamp2 mRNA level compared to CTL (Suppl. Figure 3a). The increase of expression of EEA1 and Rab7 was confirmed at the protein level specifically in CR4 cells, but not that of Rab5 or Rab11 (Fig. 3a-b). While also overexpressed at the mRNA level, RalA, RalB, Rab27a/b were not upregulated at the protein level in CR4 cells (Suppl. Figure 3b). These results could indicate that the loss of P2X4 induced no significant alteration of the transport, or fusion of MVBs, to the plasma membrane. Instead, the increase of EEA1 and Rab7 suggests a change in the transport of endosomal compartments. Since the increase in Rab7 was not associated with a decrease but rather with an increase in EVs release in CR4 cells compared to CTL (Fig. 2b), we hypothesized that this upregulation may not be solely due as a consequence of transcriptional regulation. We therefore questioned the participation of a defective endo-lysosomal fusion to the autophagosome and whether an impaired autophagy could contribute to the observed Rab7 increase in CR4 cells under hypoxia. As shown on Fig. 3c, CR4 cells grown in hypoxia demonstrated higher levels of LC3-II, p62 (median increased by 94.2%, Fig. 3e) and Rab7 (median increased by 195.6%,

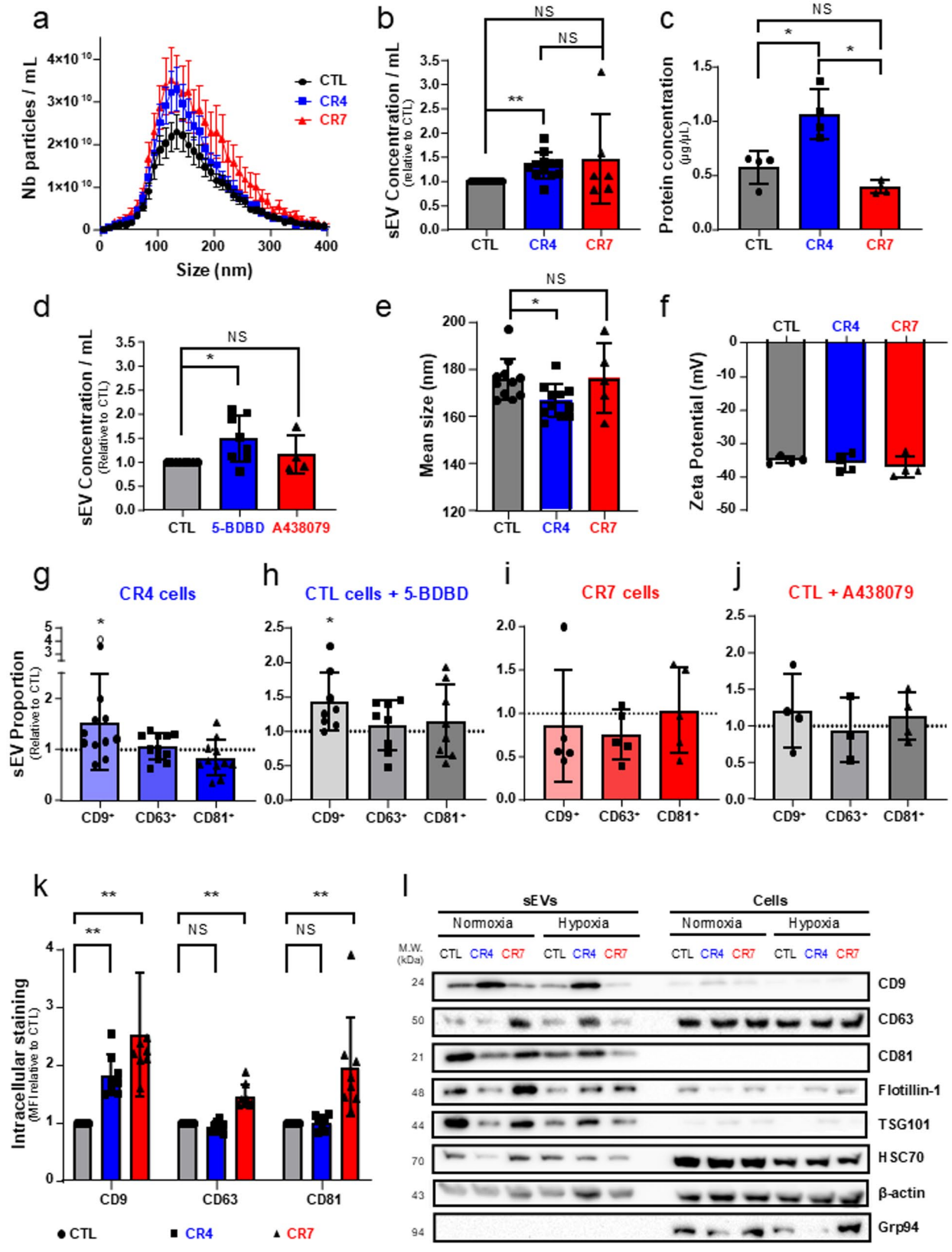

Fig. 2 (See legend on next page.)

(See figure on previous page.)

Fig. 2 Differential roles of P2X4 and P2X7 receptors in inducing sEV production under hypoxic conditions. CTL, CR4 (knock-down for the expression of P2X4) and CR7 (knock-down for the expression of P2X7) cells were grown under hypoxic conditions (1% O2) for a duration of 48 h prior to conducting analyses. **a** Size distribution and concentration of EVs purified from CTL, CR4 or CR7 cells grown under hypoxia, assessed by NTA (n = 12 independent experiments for CTL and CR4, n = 6 independent experiments for CR7). **b** Relative concentrations of sEVs per mL of supernatants, expressed relatively to that for CTL, in the same conditions than in a. The concentration of sEV produced by CR4 cells was significantly higher as compared to CTL (**, $p<0.01$). NS stands for not statistically different. **c** Protein concentrations of sEV extracts from same conditions than in a. There was a significantly higher protein concentration of sEVs extracts from CR4 cells, as compared to CTL (*, $p<0.05$) or to CR7 (*, $p<0.05$) cells. NS stands for not statistically different. **d** Relative concentration of sEVs per mL of supernatants coming from CTL cells treated with either 5-BDBD (P2X4 antagonist, 5μM) or A438079 (P2X7 antagonist, 10 μM) and expressed relatively to the CTL condition (vehicle). There was a significantly higher concentration of sEV produced by cells submitted to the P2X4 antagonist as compared to CTL (*, $p<0.05$) but not with cells treated with the P2X7 antagonist. NS stands for not statistically different. **e** Mean size (in nm) of sEVs purified from supernatants coming from CTL, CR4 or CR7 cells, in same conditions than in a. EVs produced by CR4 cells were significantly smaller than CTL (*, $p<0.05$). NS stands for not statistically different. **f** Zeta potential (in mV) of sEVs purified from supernatants coming from CTL, CR4 or CR7 cells, in similar conditions than in a. There was no difference between the three groups (n = 4 independent experiments). **g** Proportion of CD9+, CD63+ and CD81+ sEV purified from CR4 cells supernatants, assessed by Fluo-NTA, normalized to that coming from CTL cells (n = 12 independent experiments). There was a significantly higher proportion of CD9+ sEV produced by CR4 cells compared to CTL cells (*, $p<0.05$). **h** Proportion of CD9+, CD63+ and CD81+ sEVs purified from supernatants of CTL cells treated with 5-BDBD (P2X4 antagonist, 5 μM), assessed by Fluo-NTA, normalized to that coming from CTL cells (n = 8 independent experiments). There was a significantly higher proportion of CD9+ sEVs produced by cells treated with 5-BDBD (*, $p<0.05$). **i** Proportion of CD9+, CD63+ and CD81+ sEVs purified from CR7 cells, assessed by Fluo-NTA, normalized to that from CTL cells (n = 5 independent experiments). There was no statistical difference. **j** Proportion of CD9+-, CD63+- and CD81+-sEVs purified from CTL cells treated with A438079 (P2X7 antagonist, 10 μM), assessed by Fluo-NTA, normalized to that from CTL cells (n = 4 independent experiments). There was no statistical difference. **k** Intracellular expression of tetraspanins CD9, CD63, CD81 in CTL, CR4 and CR7 cells analysed by flow cytometry. Data are represented in relative MFI with mean ± SD normalized to that in 4T1 cells in CTL condition (n = 8). (**, $p< 0.01$). NS stands for no statistical difference. **l** Representative western blot showing the protein content and sEV production in CTL, CR4 and CR7 cells, under both normoxia and hypoxia. Markers of sEVs (CD9, CD63, CD81, TSG101, Flotillin1, Syntinin-1), are enriched in extracellular vesicle fractions, but not GRP94 used as a marker of endoplasmic reticulum which was only identified in total cell protein extract. sEVs produced by CR4 cells demonstrated a higher level of CD9. HSC70 and β-actin were used as control proteins

Fig. 3f) than CTL cells. The use of chloroquine (CQ) to inhibit autophagy allowed use to calculate an autophagic flux (ratio of the LC3-II level without vs. with CQ). As already reported [45], loss of P2X4 importantly impaired the autophagic flux (median decreased by 57.8%, Fig. 3d). In CR4 cells, treatment with CQ induced a small but significant increase in the p62 levels in CR4 cells (median increased by 17.4%, Fig. 3e) but no significant effect on Rab7 protein level (Fig. 3f). These results suggest that the accumulation of Rab7 in CR4 may be, at least partially, due to a preexisting defect in fusion between endo-lysosomal compartments (e.g. MVBs or amphisomes) and lysosomes, indicating a defective autophagy. To further explore this possibility, we performed immunofluorescence analyses of CD63-positive compartments in CR4 and CTL cells (Fig. 3g). We noticed a significant increase in the total number of these $CD63^+$-compartments (median increased by 156.4%, Fig. 3h) with no change in size (Fig. 3i). Similarly, there was a significant increase in the total number of $Rab7^+$-compartments (median increased by 116.2%, Fig. 3j-k), again without any size variation (Fig. 3l). Collectively, these results suggest a role for P2X4 in the degradation of a specific subpopulation of EVs through endo-lysosomal or amphisome-lysosomal fusion.

P2X4 knock-down modifies sEV proteome through secretive autophagy

To follow this hypothesis, we conducted comparative proteomic analyses from sEVs purified from CTL and CR4 cell grown under hypoxia (Fig. 4a). Proteomic analysis identified 1,209 proteins (1,032 human annotated ortholog proteins), of which 190 were significantly increased (> 1.5-fold-change) and 317 were significantly decreased (< 0.5-fold-change) in sEV coming from CR4, compared to sEV from CTL (Fig. 4b-c). Protein identified in sEVs from CTL and CR4 cells matched with the Vesiclepedia database (7,184 proteins in the group term "exosome", the full list encompassing 8,548 proteins) at 91.6% (890 out of 972) and 92.0% (81 out of 936), respectively (Fig. 4c). Similarly, significantly differentially expressed proteins (increased level > 1.5-fold-change) identified in sEV matched with Vesiclepedia database at 90.3% (271 out of 300) for CTL and 88.8% (166 out of 187) for CR4 (Fig. 4d). Row clustering analysis was performed with proteins identified in sEVs from CTL and CR4 cells. Z-scores from precursor intensities are visualized as a heatmap (Fig. 4e). This analysis revealed several clusters of differentially expressed proteins, consistently observed across biological triplicates. We further analysed cellular components and signalling pathways to which belong identified proteins. For this aim, we used the murine database (Suppl. Figure 4a-e). However, the murine database is less comprehensive than the human one. Therefore, we also used human orthologs protein markers. Gene Ontology (GO) term analysis (Cellular Component, CC) revealed that enriched proteins identified in sEVs from CTL and CR4 originate from the "Extracellular vesicles / exosome" (at 62.35% and 62.24% of markers, respectively), from the "cytosol" (61.17% and 62.24%, respectively), from the "cytoplasm" (48.33% and 49.59%, respectively), from the "plasma membrane" (48.33% and 45.95%, respectively) or from the "nucleus" (36.79% and 38.07%, respectively) (Fig. 4f).

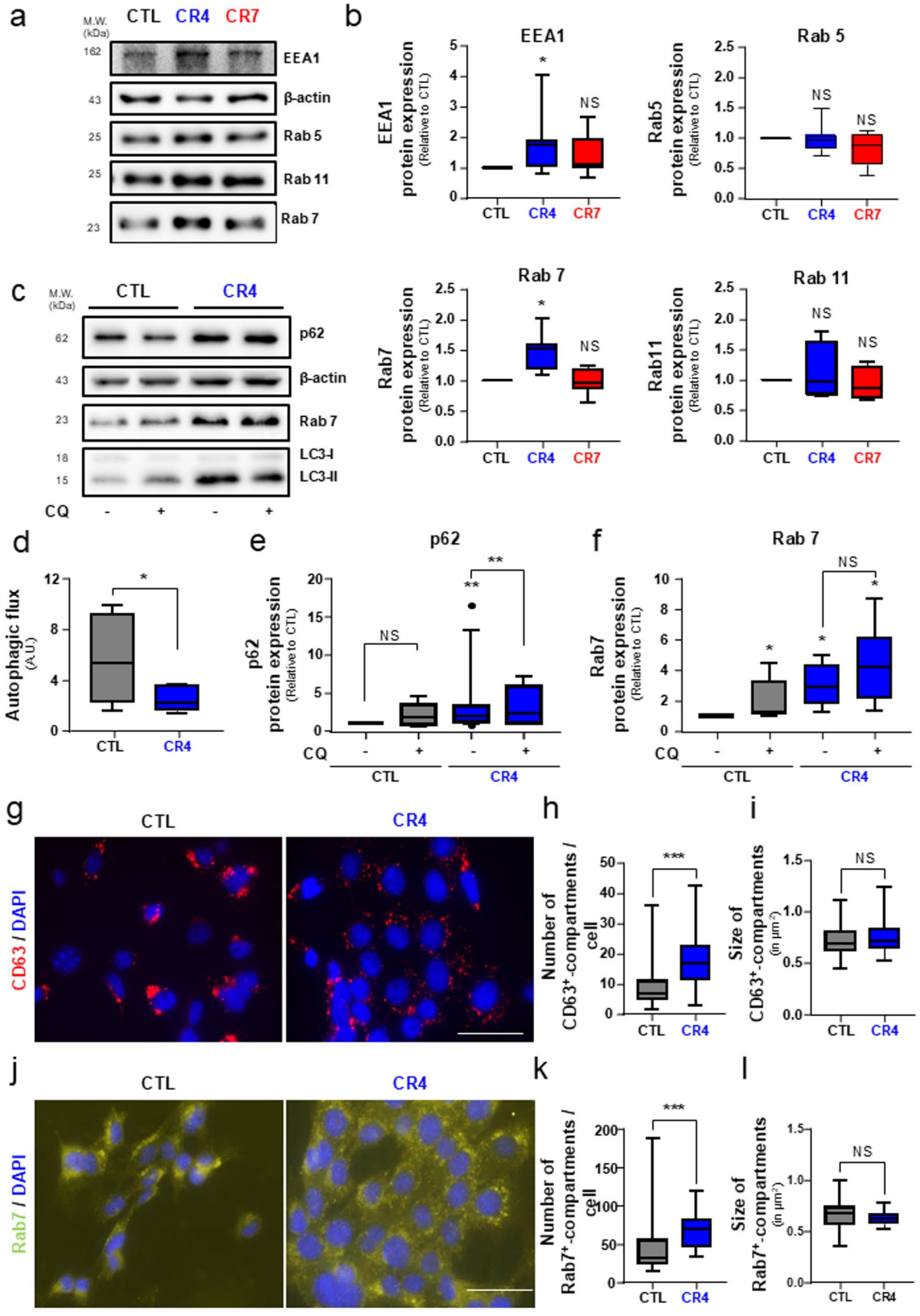

Fig. 3 (See legend on next page.)

(See figure on previous page.)

Fig. 3 P2 4 and P2X7 receptors differentially control the expression of Rab GTPases and proteins involved in vesicle and endo-lysosomal trafficking. **a** Representative western blots showing the expression of EEA1, Rab5, Rab7 and Rab11 proteins in CTL, CR4 and CR7 cells grown under hypoxic conditions. β-actin was used as a control loading protein. **b** Quantification of EEA1 (upper left), Rab5 (upper right), Rab7 (lower left) and Rab11 (lower right) proteins from experiments shown in a. Proteins levels are expressed relatively to that of β-actin and to the CTL cell line ($n = 4$–8 independent experiments, *, $p < 0.05$, NS stands for no statistical difference to the CTL cell line). **c** Representative western blots showing the expression of p62, Rab 7 and LC3-I and LC3-II proteins in CTL and CR4 cells cultivated under hypoxia and with or without treatment with chloroquine (CQ, 100 µM) for 6 h. **d** Autophagic flux in CTL and CR4 cells calculated from experiments shown in c, as being the ratio (LC3-II/β-actin in the presence of CQ)/(LC3-II/ β-actin in the absence of CQ). ($n = 8$ independent experiments, *, $p < 0.05$). **e** Relative quantification of p62 protein levels in CTL and CR4 cells, grown in hypoxia, as from experiments shown in c. P62 levels are expressed relatively to that of β-actin and to the CTL cell line in the absence of CQ ($n = 12$ independent experiments, **, $p < 0.01$, NS stands for no statistical difference). **f** Relative quantification of Rab7 protein levels in CTL and CR4 cells, grown in hypoxia, as from experiments shown in c. Rab7 levels are expressed relatively to that of β-actin and to the CTL cell line in the absence of CQ ($n = 7$ independent experiments; *, $p < 0.05$, NS stands for no statistical difference). **g** Fluorescence imaging showing nuclei (blue staining DAPI) and illustrating the expression of CD63 (red staining) in CTL and CR4 cells. Scale bar, 75 µm. **h** Quantification of the number of $CD63^+$ compartments in CTL and CR4 cells from images as in g. ($n = 35$–37 images from 3 independent experiments, ***, $p < 0.001$). **i** Quantification of the size of $CD63^+$-compartments in CTL and CR4 cells from images as in g. ($n = 35$–37 images from 3 independent experiments, NS stands for no statistical difference). **j** Fluorescence imaging showing nuclei (blue staining DAPI) and illustrating the expression of Rab7 (green staining) in CTL and CR4 cells. Scale bar, 75 µm. **k** Quantification of the number of $Rab7^+$- compartments in CTL and CR4 cells from images as in j. ($n = 36$ images from 3 independent experiments, ***, $p < 0.001$). **l** Quantification of the size of $Rab7^+$-compartments in CTL and CR4 cells from images as in j. ($n = 36$ images from 3 independent experiments, NS stands for no statistical difference)

These analyses suggest exosomal origin of sEV purified from CTL and CR4 cells, along with a possible subpopulation of small ectosomes as evidenced by the presence of plasma membrane proteins, though overlap between categories is known. The percentage of protein markers present in this different CC category did not reveal difference between samples from CTL and CR4 cells. GO analysis on Biological Processes (BP) using human orthologs showed the enrichment in categories such as "Signal transduction" (10.95% and 10.89%), "cell adhesion" (7.56% and 6.98%), "chromatin remodelling" (6.46% and 6.13%) or "Positive regulation of gene expression" (5.37% and 4.97%) in CTL and CR4 respectively. Interestingly, we also found BP related to cancer cell aggressiveness susceptible to predict the effect of these sEV on recipient cells, such as: "Negative regulation of apoptotic process" (5.81% and 5.60%, respectively), "Positive regulation of cell migration" (5.26% and 4.86%, respectively) or "Positive regulation of cell proliferation" (4.60% and 4.12%, respectively) (Fig. 4g). Nevertheless, this analysis did not identify any significant difference between CTL and CR4. Similar results were obtained using murine database (Suppl. Figure 4d). The specific analysis of differentially expressed human orthologs in sEV (> 1.5-fold change) in BP indicated proteins associated with "Signal transduction", "Cell migration" and "Cell adhesion", with a higher proportion of these proteins in sEVs from CR4 cells compared to CTL cells (Fig. 4h). Similar results were obtained using murine databases and GO terms BP relative to "endocytosis", "Cell adhesion" and "Cell migration", again with higher proportion for sEVs of CR4 cells (Suppl. Figure 4e). These results support the hypothesis that P2X4 knock-down alters sEV protein composition in ways that may affect recipient cancer cell behaviour, particularly in terms of migration and invasion.

We previously reported that silencing P2X4 in 4T1 cells led to reversion of epithelial-to-mesenchymal transition (EMT) [45]. Interestingly, proteomic analysis revealed the upregulation of epithelial markers such as E-cadherin (Log2 FC (ref=4T1): 1.08), ZO-2 (Log2 FC (ref=4T1): 0.928), Epcam (Log2 FC (ref=4T1): 2.5) and the down-regulation of mesenchymal markers such as vimentin (Log2 FC (ref=4T1): -8.37) and Col6a1 (Log2 FC (ref=4T1):-0.511) in sEV from CR4 cells compared to that from CTL cells (Suppl. Table 1). To investigate the involvement of P2X4 on endoso-lysosomal transport and fusion, and its consequences on sEV biogenesis, we used the differential protein list (> 1.5-fold change) from sEV of CTL and CR4 cells to interrogate GO website provided by PANTHERs (see Materials and methods section), using the key words "exosome", "autophagy", "endosome", "multivesicular bodies" and "lysosome". All significant GO terms ($p < 0.05$) are listed in Suppl. Figure 5a-b. Interestingly, only sEVs from CTL showed GO terms related to endosome/MVB transport or fusion with lysosomes :"endosome transport via multivesicular body sorting pathway" (GO:0032509); "multivesicular body-lysosome fusion" (GO:0061763); "late endosome to vacuole transport via multivesicular body sorting pathway" (GO:0032511) indicating that proteins involved in these processes were either downregulated or absent in sEVs from CR4 cells. Conversely, only the CR4 list displayed GO terms related to: "positive regulation of extracellular exosome assembly" (GO:1903553), "autophagosome maturation" (GO:0097352), "protein targeting to vacuole involved in autophagy" (GO:0071211), indicating the release of autophagic proteins in sEV from CR4 cells. Therefore, these results suggested an autophagy-dependent unconventional mode of exosome secretion, potentially via amphisome secretion [20]. All proteins from the list associated with these GO terms were compiled, and Z-scores among replicates were calculated and visualized as heatmaps (Fig. 5a-c). While some redundancy was observed, expression trends were consistent across

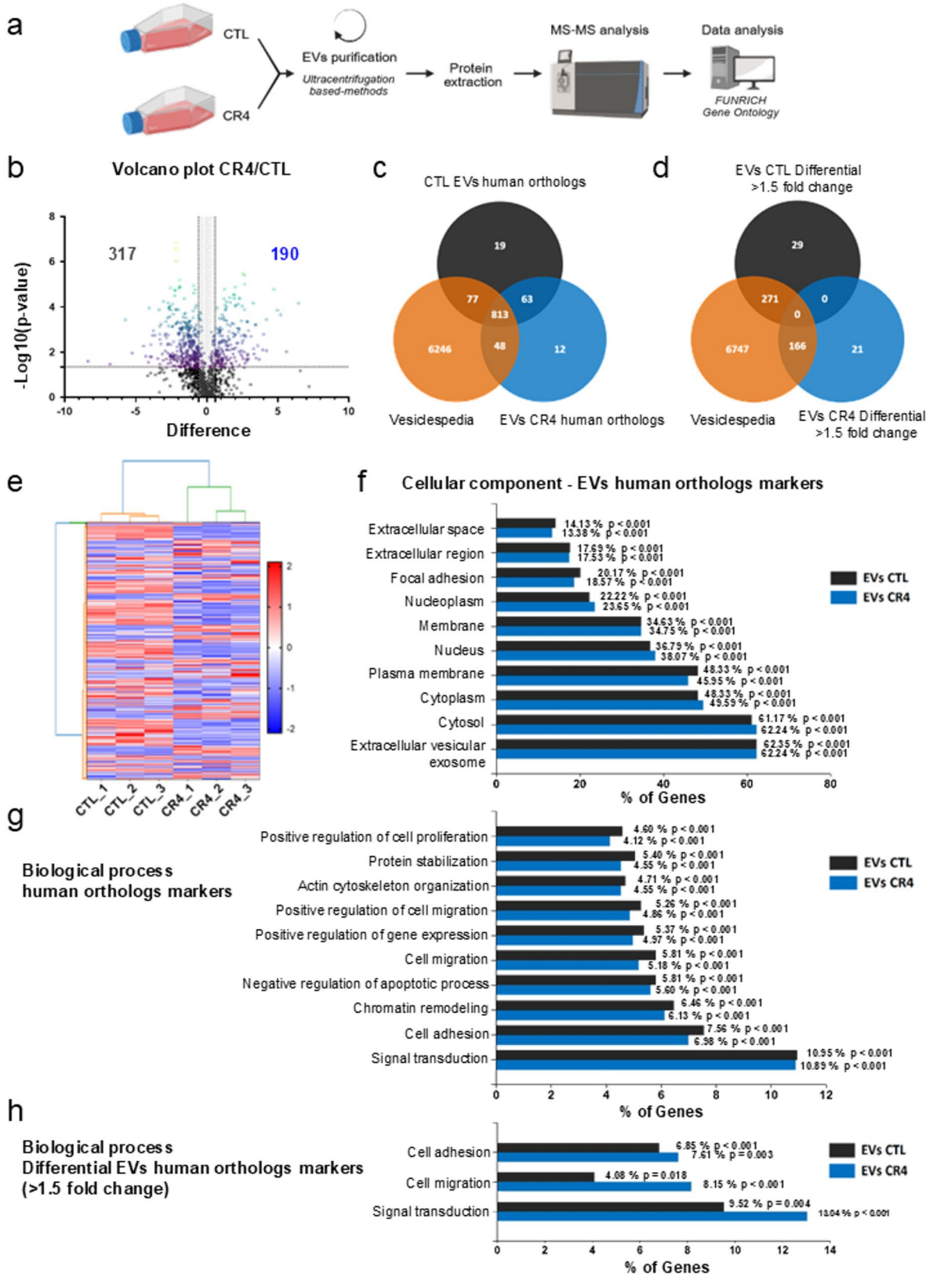

Fig. 4 (See legend on next page.)

(See figure on previous page.)

Fig. 4 Proteomic analysis of EVs released by CTL or CR4 cells cultivated in hypoxia and purified using ultracentrifugation. **a** Schematic representation of the methodology used to analyse the proteomic content of EVs produced by CTL or CR4 cells. Cells were grown in hypoxia and EVs released in the supernatants were purified by ultracentrifugation-based methods, proteins were purified and analysed by MS-MS spectrometry. Sequences were analysed using the FUNRICH gene ontology tool. **b** Volcano plot illustrating quantitative differences in protein expression between EVs from CTL and CR4 cells. Dots above the threshold line represent proteins with statistically significant differences (p-value < 0.05). A total of 190 proteins were upregulated and 317 downregulated in EVs from CR4 compared to those from CTL. **c** Venn diagrams showing total human orthologs proteins identified in EVs from CTL and CR4 cells, and from the Vesiclepedia database. **d** Venn diagrams showing the differential expression of human orthologs proteins (level of expression > 1.5-fold change) identified in EVs from CTL and CR4 cells, and from the Vesiclepedia database. **e** Heatmap illustrating the differential protein expression analysis (z-score) of all proteins identified in EVs from of CTL and CR4 cells ($n = 3$ independent analyses showing similarities in biological replicates). **f** Representation of cellular component origin of human ortholog proteins identified from EVs released from CTL (black bars) and CR4 (blue bars) cells. Analysis was performed using FunRich with the Gene Ontology data base, indicating a majority of proteins classically expressed in extracellular vesicles and exosomes. **g** Representation of biological processes involving human ortholog proteins identified in EVs released from CTL (black bars) and CR4 (blue bars) cells. Analysis was performed using FunRich with the Gene Ontology data base. **h** Representation of biological processes involving human ortholog proteins which expression levels showing a > 1.5-fold change, identified in EVs released from CTL (black bars) and CR4 (blue bars) cells. Analysis was performed using FunRich with the Gene Ontology data base

replicates. Importantly, components of the ESCRT complex (e.g., Chmp1b2, Chmp1a, Chmp4, Mvb12a and Vps) were downregulated in CR4 sEVs. STRING-based interactome analysis of these downregulated proteins revealed strong predicted functional interactions, further suggesting impaired late endosome/MVB-lysosome fusion (Fig. 5b). In contrast, autophagy-related proteins such as Sqstm1/p62 and GABARAPL2, and proteins targeting compartment to the autophagosome (Snap29, Chmp5, Lamp2, Hspa8), were upregulated in sEV from CR4 cells (Fig. 5c), further confirming altered amphisome-lysosome fusion and defective autophagy, in line with previous results (Fig. 3d). We also observed the increase of syndecan-1 (Sdc1) and syndecan-4 (Sdc4), two heparan sulfate proteoglycans involved in exosome biogenesis [56], in sEV from CR4 cells, consistent with the increase of sEVs release (Fig. 2). Also, proteins implicated in the regulation of early endosome transport to late endosome (Rab5b/c, Chmp5, Rdx, Msn) were upregulated in sEV from CR4 cells. Interactome analysis of these proteins upregulated in sEVs from CR4 cells, mostly identified functional interactions between actors of exosome assembly and that of autophagy and autophagosome maturation (Fig. 5d). The accumulation of autophagic and early endosome markers in sEV from CR4 cells might result from an impaired degradation rather than from an active inclusion. Western blotting experiments confirmed the increase of p62 and LC3-II levels in sEV from CR4 cells compared to CTL and CR7 cells under hypoxia (Fig. 5e).

P2X4 expression in donor cancer cells modulates invasion of recipient cancer cell

We next assessed the consequences of these changes in the production and proteomic content of sEV on recipient CTL cells. As previously, we purified sEV from CTL, CR4 and CR7 cells grown under hypoxia, and labelled them with the fluorescent PKH67 membrane probe. Integration of these sEVs in recipient CTL cells after 4 h was confirmed by epifluorescence microscopy (Fig. 6a). This integration was qualitatively evaluated by flow cytometry and a ratio of mean fluorescence intensity (MFI) was calculated by comparing the MFI after 4 h to that after 1 h incubation with PKH67-stained sEV (concentration equivalent to 20 µg proteins /mL). Interestingly, sEV purified from CR4 cells demonstrated a faster capacity of integration than those from CTL or CR7 cells (Fig. 6b). These functional results were somehow in line with proteomic data (Fig. 4g-h and Suppl. Figure 4e). We then developed a co-culture assay between donor cells expressing (CTL) or not P2X4 (CR4) or P2X7 (CR7), and CTL recipient cancer cells under hypoxic conditions (Fig. 6c). CTL recipient cells co-cultured with CR4 donor cells showed a significant reduction in invasive capacities compared to those co-cultured with CTL donor cells (median reduced by 35%). By comparison, co-culture with CR7 cells induced no change in invasive capacities of CTL recipient cells (Fig. 6d). Furthermore, the use of GW4869, a n-SMase2 inhibitor acting as a blocker of the ESCRT-independent exosome biogenesis, significantly reduced the invasive capacities of recipient CTL cells co-cultured with either CTL or CR7 donor cells, but not that of cells co-cultured with CR4 cells (Fig. 6d). These results were not observed under normoxia (Suppl. Figure 6a) and sEVs coming from the three cell lines had no effect on recipient cells survival either in normoxia or in hypoxia. These results strongly suggest that P2X4 contributes to sustain or increase the invasive capacities of distant cancer cells under hypoxia, through the release of pro-invasive sEVs.

Discussion

The P2X7 receptor has garnered significant attention in cancer research over the past two decades due to its complex and sometimes contradictory role in tumour progression, raising questions about whether pharmacologically targeting it would be beneficial or detrimental [57, 58]. On one hand, P2X7 has been demonstrated to support primary tumour growth [22, 32] and progression [33–35]; on the other hand, it has been involved in

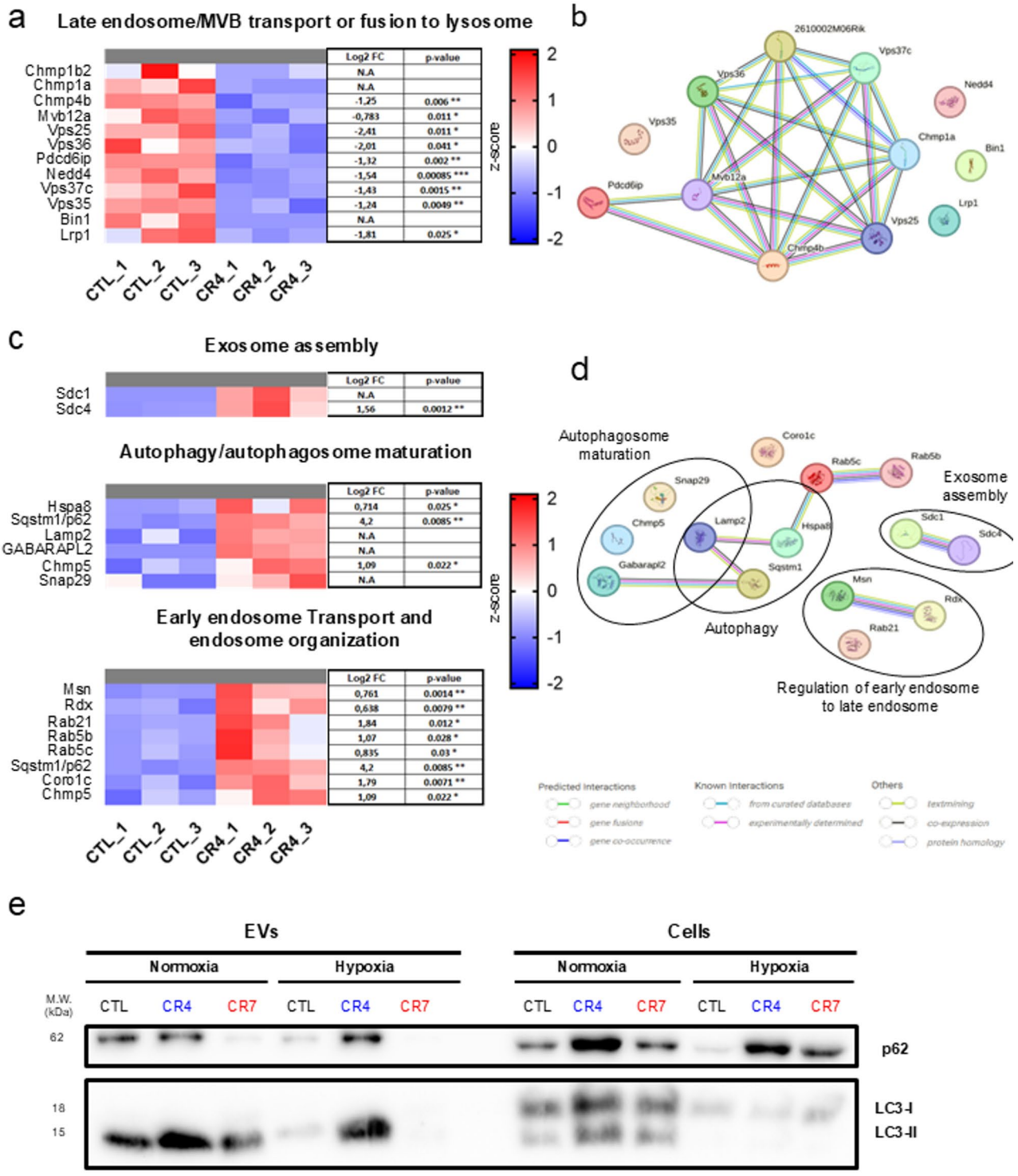

Fig. 5 (See legend on next page.)

both basal [59] and chemotherapy-induced anti-tumour immune responses [60]. This receptor which is crucial for the initiation of the NLRP3 inflammasome/caspase-1/IL-1β and IL-18 inflammatory cascade [37] has also been implicated in promoting tumour-associated inflammation [36]. The P2X7 receptor has long been known to participate in microvesicle shedding from immune cells [38–40, 61], microglial [62] as well as to participate in mediating the release EVs under various pathophysiological conditions [63], including cancers

(See figure on previous page.)

Fig. 5 EVs from P2X4-deficient cells show a differential expression of proteins involved in endo-lysosome, exosome and autophagosome fusion and maturation. **a** Heatmap illustrating the differential expression (z-score, differences in Log2-fold change and p value) of proteins implicated in late endosome/MVBs transport and fusion to lysosome (GO term reported Supplementary Fig 5b), identified in EVs coming from CTL and CR4 (n=3 independent experiments). *, $p < 0.5$; **, $p < 0.01$; ***$p < 0.001$. **b** STRING analysis showing the interaction of selected proteins identified as being upregulated in EVs from CTL cells, thus expressing P2X4, and involved in late endosome/MVBs transport or fusion to lysosome. **c** Heatmap illustrating the differential expression (z-score, differences in Log2-fold change and p value) of proteins involved in early endosome transport, endosome maturation, autophagy and exosome assembly (GO term reported Supplementary Fig 5a), identified in EVs coming from CTL and CR4 (n=3 independent experiments). Statistically different at: *, $p < 0.5$; **, $p < 0.01$ and ***, $p < 0.001$. **d** STRING analysis showing the interaction of selected proteins identified as being upregulated in EVs from CR4 cells, thus not expressing P2X4, involved in exosome assembly, autophagy and early endosome transport, endosome maturation. **e** Representative western blot showing the presence of autophagy markers LC3-II and P62 in CTL, CR4 and CR7 cells, cultivated either under normoxia or hypoxia, and their respective purified EVs

[41, 64], where it promotes the secretion of pro-metastatic exosomes [41]. Its closely related family member, the P2X4 receptor, has also gained interest in carcinoma research due to a more consistently reported role in promoting metastatic progression [43–45]. The P2X7 receptor is functionally expressed at the plasma membrane of cancer cells [33–35], whereas P2 4 is primarily localized in endo-lysosomal compartments and regulates the fusion of lysosomes with autophagosomes and/or the plasma membrane in response to environmental metabolic pressure [45]. P2X4 thus supports autophagy and may also influence EV release, as shown in HCV-infected hepatocytes [46]. This study aimed to investigate the roles of P2X4 and P2X7 in the release of small EVs (sEVs), including exosomes, under hypoxic conditions, a key aspect of the tumour microenvironment that promotes cancer progression.

Previous studies have demonstrated the involvement of P2X7 in mammary cancer cell aggressiveness [33–35] and its participation to exosome release from cancer cells [41, 64]. However, in our study, neither silencing P2X7 nor selective pharmacological inhibition altered sEV release, which contradicts earlier findings using less selective pharmacological antagonists such as KN62 [64]. Although P2X7 was confirmed to be functional at the plasma membrane [35] (Suppl. Figure 1c), stimulation with ATP or BzATP over 24 h at non-toxic concentrations did not enhance sEV release. In contrast, other studies used much higher ATP concentrations (3–5 mM) for shorter durations (30–90 min) [41]. These discrepancies may be due to differences in the subtype of released EVs, receptor expression levels, or even cell-type specific responses.

In earlier studies, P2X4 knock-down or inhibition in cancer cells reversed EMT by decreasing vimentin and increasing E-cadherin, leading to changes in cell morphology and invasiveness [44, 45]. In this study, we demonstrated that P2X4 knock-down not only reduced the invasive capacity of cancer cells expressing P2X4 but also affected neighbouring co-cultured cells. Proteomic analysis of sEVs from P2X4-deficient cells revealed increased abundance of epithelial markers (E-cadherin, ZO-2, EpCAM) and reduced levels of mesenchymal markers (vimentin, Col6a1), consistent with the known cellular origin signatures of EVs [65]. Interestingly, sEVs from P2X4 knock-down cells, while less effective at transferring invasive traits to recipient cells, were integrated more rapidly. This was associated with increased release of $CD9^+$ sEVs under hypoxia. CD9 is known to facilitate EV integration in recipient cells [66], possibly explaining this observation. However, the mechanism by which P2X4 restrains $CD9^+$ sEV release remains unknown. Furthermore, we demonstrated that treatment with the cell-permeable neutral sphingomyelinase (nSMase) inhibitor GW4869 counteracted the effect of P2X4 on small extracellular vesicle (sEV) release. GW4869 is well established to inhibit EV biogenesis by targeting the ESCRT-independent pathway, notably through interference with ceramide-dependent processes within endosomal lipid raft domains. At this stage, however, we have no evidence indicating that P2X4 also modulates the ESCRT-dependent pathway involved in multivesicular body (MVB) biogenesis.

Our results demonstrate that genetic knockdown or pharmacological inhibition of intracellular P2X4 alters endo-lysosomal trafficking and autophagic activity, thereby modulating small extracellular vesicle (sEV) release. In the present study, as well as in our previous work [45], we showed that P2X4 is strictly localized to endo-lysosomal compartments in mammary cancer cells. This finding is consistent with earlier reports in other cell types [42]. Given this intracellular localization, stimulation with extracellular ATP did not affect sEV release or composition. The subcellular distribution of P2X4 likely restricts its accessibility to exogenous ATP. These observations contrast with findings by Kim et al. [46] in HCV-infected hepatocytes, where high concentrations of extracellular ATP enhanced $CD63^+$ exosome release. Our data support the notion that P2X4 is functionally active within intracellular compartments and can be antagonized by a lipophilic, cell-permeant inhibitor such as 5-BDBD. In this context, receptor activation would depend on the availability of agonists within the intraluminal environment. It has been proposed that endo-lysosomal luminal compartments may contain ATP at concentrations sufficient to activate P2X4,

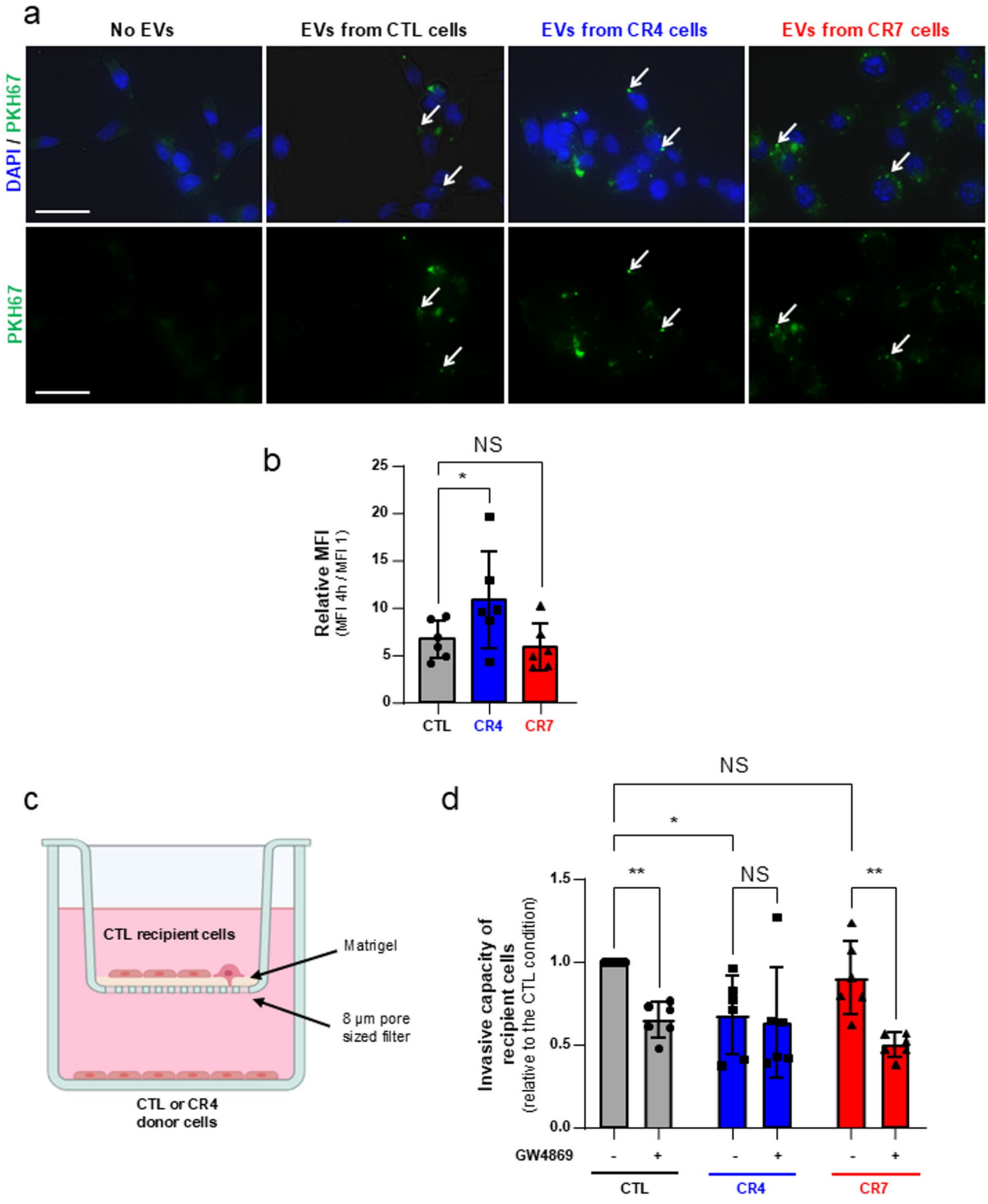

Fig. 6 (See legend on next page.)

(See figure on previous page.)

Fig. 6 sEVs produced from P2X4-expressing cancer cells enhance the invasive capacities of recipient cancer cells. **a** CTL cancer cells were treated with EVs purified from CTL, CR4 or CR7 cells, grown under hypoxic conditions (1% O2). EVs were stained with green, fluorescent membrane probe PKH67. Representative fluorescent images obtained after 4 h treatment with 20 µg/mL of EVs. Upper, merged images showing DAPI staining for identification of cell nuclei and PKH67 staining showing EVs. Lower, PKH67 staining alone. White arrows indicate EVs incorporated into CTL recipient cells. Scale bars, 75 µm. **b** Assessment of the uptake as a function of time of PKH67-stained EVs, produced by CTL, CR4, CR7 cells, in CTL cancer recipient cells by flow cytometry (treatment with 20 µg/mL EVs protein). Results indicate a speed of uptake expressed as a ratio of the uptake after 4-h on that after 1-h incubation. Data are represented in rMFI with Mean MFI 4 h normalized to their respective control MFI 1 h, mean ± SD (n = 6 independent experiments). *, indicate a statistical difference at $p < 0.05$. NS stands for no statistical difference. **c** Cartoon of the experimental procedure of co-culture assays to assess cell invasiveness performed in hypoxic conditions (1% O2). Invasiveness of recipient CTL was assessed as being their capacity to invade an 8 µm-sized filter covered by a thin layer of Matrigel. These cells were co-cultured with CTL, CR4, CR7 donor cells seeded at the bottom of the well. **d** Invasive capacities of recipient CTL cells co-cultured with CTL, CR4 or CR7 donor cells, as illustrated in c. Experiments were performed in the absence (vehicle, DMSO) or presence of the nSMAse inhibitor GW4869 (10 µM). Data are normalized to the control condition, in absence of GW4869, and presented as mean ± SD ($n = 6$ independent experiments). *, $p < 0.05$ and **, $p < 0.01$. NS stands for no statistical difference

albeit at submaximal levels [67]. However, P2X4 activity is also regulated by luminal pH and is inhibited under acidic conditions [68]. Therefore, activation of P2X4 within endo-lysosomal compartments may require transient increases in luminal pH during vesicular trafficking and fusion events, potentially mediated by vacuolar H^+-ATPase (V-ATPase) activity [69].

Our proteomic data clearly indicate that the loss of P2X4 in cancer cells induced the downregulation of key proteins involved in endo-lysosomal fusion (Chmp1b2, Chmp1a, Chmp4, Mvb12a and Vps) in sEVs, concomitantly with the increase of autophagic markers (LC3-II and p62), characteristic of an "autophagy-dependent unconventional exosome secretion", also referred as "secretive autophagy". Amphisomes, formed by the fusion of autophagosomes with MVBs, can release their content via plasma membrane fusion [70]. In this context, the use of chloroquine or bafilomycin, which blocks endo-lysosomal fusion, increases amphisome formation and the release of autophagy marker-containing sEVs [71].

This type of secretion, defined by markers such as CD9, p62 and LC3-II, aligns with our findings following P2X4 inhibition or knockdown [72]. While the biological implications of this secretory autophagy in cancer remain unclear, it may contribute to processes like metastatic niche preparation [18] or angiogenesis [72]. Notably, our study suggests that this secretory autophagy, induced by P2X4 knock-down, may instead exert anti-invasive effects. There is conflicting opinion about the role of Rab7 in endosomal trafficking. It has been proposed a role for Rab7 in late endosome or autophagosome trafficking to lysosome, leading to exosome degradation [73], while others studies attest to a role in MVBs transport towards the plasma membrane and exosome release [55, 74]. We observed an increase in the Rab7 level in CR4 cells, which exhibits reduced autophagic flux. Chloroquine treatment did not further elevate Rab7, supporting the hypothesis of a compensatory response to autophagy inhibition [75]. However, we could not conclusively determine whether P2X4 modulates fusion of lysosomes with amphisomes or MVBs, which requires further study.

In conclusion, this study has identified a specific role for P2X4 in regulating Rab7-dependent endo-lysosomal trafficking and the associated release of pro-invasive $CD9^+$ sEVs through an autophagy-related secretory pathway. P2X4 appears to contribute to the biogenesis of pro-invasive sEVs that may promote mammary cancer progression and metastasis.

Supplementary Information

The online version contains supplementary material available at https://doi.org/10.1186/s12964-026-02811-5.

Supplementary Material 1.

Supplementary Material 2. Suppl. Fig. 1: (a) Representative epifluorescence imaging performed on 4T1 CTL cells, identifying the expression level of P2X4 (red staining) in intracellular compartments, with no apparent co-localization with the plasma membrane (green staining, WGA-AlexaFluor 488). Cell nucleus was stained with DAPI (blue staining). Scale bar, 10 µm. (b) P2rx4 and P2rx7 expression levels assessed by RT-qPCR in CR4 and CR7 cells and expressed relatively to CTL cells. NS, stands for no statistical difference. Statistical differences at ***, p<0.001; * p<0.05. (c) Cellular electrophysiology experiments (patch clamp) showing inward, non-desensitizing, currents in response to 10 s-long application of 3 mM ATP in CTL cells at a holding potential of -60 mV, but not in CR7 cells knocked-down for the expression of P2rx7. (d) Relative concentration of sEVs per mL of supernatants coming from CTL cells treated with either 5-BDBD (P2X4 antagonist, 5µM) or A438079 (P2X7 antagonist, 10 µM) in normoxia and expressed relatively to the CTL condition (in presence of vehicle). n= 4-8 independent experiments. NS, stands for no statistical difference. (e) Proportion of CD9+-, CD63+- and CD81+-sEVs purified from supernatants of CTL cells treated with 5-BDBD (5 µM) under normoxia, assessed by Fluo-NTA, normalized to that coming from CTL cells (n=8 independent experiments). NS, stands for no statistical difference. (e) Proportion of CD9+-, CD63+- and CD81+-sEVs purified from supernatants of CTL cells treated with A438079 (10 µM) under normoxia, assessed by Fluo-NTA, normalized to that coming from from CTL cells (n=3 independent experiments). There was no statistical difference.

Supplementary Material 3. Suppl. Fig. 2: (a) Number of sEVs released per cells in the supernatants, from the three cell types (CTL, CR4 and CR7) grown either under normoxia (N) or hypoxia (H), assessed by NTA (n = 7-8 independent experiments in each condition). N.S. stands for not statistically different. #, indicates a significant difference at p<0.05 between CTL normoxia and CR4 normoxia. *, indicates a significant increased difference at p<0.05 between CTL hypoxia and CR4 hypoxia. (b) Median size of purified sEVs, from CTL and CR7 cells grown either under normoxia (N) or hypoxia (H), assessed by NTA (n = 7-8 independent experiments in each condition). N.S. stands for not statistically different. (c) Immunodetection of intracellular of tetraspanins CD9, CD63 and CD81 assessed by flow cytometry in CTL, CR4 and CR7 cells under hypoxia, treated or not with 100 µM extracellular ATP treatment for 48h. Data are represented in relative MFI to the CTL condition without ATP and are expressed as

mean ± SD (n = 3 independent experiments). No statistical difference was observed under ATP treatment. (d) Similar experiments as in a) were performed in CTL, CR4 and CR7 cells under hypoxia treated or not with 300 µM extracellular BzATP treatment. Data are represented in relative MFI to the CTL condition without BzATP and are expressed as mean ± SD (n = 3 independent experiments). No statistical difference was observed under BzATP treatment. (e) Proportion of total, CD9+-, CD63+- and CD81+- sEVs assessed by Fluo-NTA, from EVs purified from supernatants of CTL cells grown in hypoxia and stimulated or not with 30 µM extracellular ATP for 48h. Results are presented relatively to the CTL condition without ATP (n=3 independent experiments). No statistical difference was observed under ATP treatment. (f) Proportion of total, CD9+-, CD63+- and CD81+- sEVs assessed by Fluo-NTA, from EVs purified from supernatants of CR4 cells grown under hypoxia and stimulated or not with 30 µM extracellular ATP for 48h. Results are presented relatively to the CR4 condition without ATP (n=3 independent experiments). No statistical difference was observed under ATP treatment. (g) Proportion of total, CD9+-, CD63+- and CD81+- sEVs assessed by Fluo-NTA, from EVs purified from supernatants of CR7 cells grown in hypoxia and stimulated or not with 30 µM extracellular ATP for 48h. Results are presented relatively to the CR7 condition without ATP (n=3 independent experiments). No statistical difference was observed under ATP treatment.

Supplementary Material 4. Suppl. Fig. 3: (a) RT-qPCR experiments indicating the mRNA expression of Rab GTPases, Lamp1/2 and EEA1 genes in CR4 and CR7 cells comparatively to CTL cells, under hypoxia. Results are coming from 5 independent experiments. Statistical differences at **, $p<0.01$; * $p<0.05$. (b) Representative western blot of Rab27a, Rab27b, Ral A, Ral B in CTL, CR4 and CR7 cells cultivated under hypoxia.

Supplementary Material 5. Suppl. Fig. 4: Proteomics analysis of sEVs purified, by ultracentrifugation-based methods, from supernatants of CTL and CR4 cells grown under hypoxia. Venn diagrams showing a) total and b) differential (>1.5 fold-change) murine proteins, using the Vesiclepedia murine database. c) cellular components and d) biological process analysis of murine proteins in sEVs coming from CTL and CR4 cells, performed with FunRich using Gene Ontology database. e) biological process analysis of differential murine protein of CTL and CR4 cells (>1.5-fold change).

Supplementary Material 6. Suppl. Fig. 6: a) Invasive capacity of recipient CTL cells co-cultured with CTL, CR4 or CR7 donor cells in normoxic condition, in presence or absence of GW4869 (10 µM). Data are normalized to CTL in absence of GW4869 (vehicle) (n = 2). b) effect of sEV treatment on recipient cell viability. sEV were purified from CTL, CR4 or CR7 cells cultivated in either normoxia or hypoxia. Recipient CTL cells were treated with 50,000 sEV per cells during 72h.

Supplementary Material 7. Suppl. Fig. 7: Full uncropped Gels and Blots images of western blots presented in regular or supplementary figures.

Supplementary Material 8.

Supplementary Material 9.

Acknowledgements
We thank Mrs Carole Desplanches and Mrs Sylvie Poguet for secretarial and administrative assistance and all members of the Inserm UMR1327 ISCHEMIA research unit for fruitful scientific discussions. We thank Mrs Hasna Djermouni and Svetlana Uzbekova for discussions on proteomics analyses. We thank David Pragout and Emma Créteur, as well as former master students in the lab. We thank Ms Louhanne Claudepierre for validation of qPCR primers. Electron microscopy data were obtained with the assistance of the IBiSA Electron Microscopy Facility of the University of Tours as a part of the Inserm US61, and we are grateful to M. Julien Burlaud-Gaillard for his help. T.D., M. E., A. H.-M., S.C., L.-H.J. and S.R. are active members of the European COST Action CA21130 "P2X receptors as a therapeutic opportunity (PRESTO)". On the PIXANIM platform (Imaging facility for phenotyping, from animal to molecule, https://doi.org/10.17180/CQ4D-DW26), the high resolution mass spectrometer (Orbitrap) was financed (SMHART project, 35069) by the European Regional Development Fund (ERDF), the Conseil Régional du Centre, the French National Institute for Agricultural Research and Environment (INRAE) and the French National Institute of Health and Medical Research (Inserm).

Authors' contributions
All authors contributed extensively to the work presented in this study. T.D. performed cell culture, molecular and cellular biology experiments, sEV isolation and characterization, assessed cell viability and invasion, immunofluorescence imaging, flow cytometry, proteomic and statistical analyses, analysed data and wrote the manuscript. M.E. and J.G. performed cell culture, sEV isolation and characterization, western blotting experiments. A.H.-M. participated to cell culture, sEVs isolation and performed electron microscopy experiments. A.V.V.D.S. participated in cell culture and immunofluorescence imaging. R. L. participated in flow cytometry analyses. S.C. created CRISPR cell lines and participated in autophagy analyses with C.T. V.L., A.-P.T. and D.T., conducted proteomic analyses at the PIXANIM platform. V.C. participated in proteomic analyses. L.F. performed cell culture, sEV isolation and western blotting experiments. G.Y., C.B. and L.-H.J. brought scientific input and participated to critical reading of the manuscript. S.R. directed the research, obtained funding, designed the study, analysed the data and wrote the manuscript.

Funding
This work was supported by the "Ministère de la Recherche et des Technologies", the Région Centre-Val de Loire (grant "CanalEx" to S.R.), the Ligue Nationale Contre le Cancer – Interrégion Grand-Ouest (cd36, cd37, cd49, to SR) and the Institut National du Cancer (grant INCA_16110 "PURINO4EXO" to S.R.). S.R. was recipient of a prize "Prix Ruban Rose Avenir 2017" from the charity "le Cancer du sein: parlons-en!". T. D. was recipient of a PhD grant from the Région Centre-Val de Loire. M. E. was recipient of a post-doctoral grant from the Institut National du Cancer and S.C. of a grant from the Fundation Lefoulon Delalande. L-H.J. and G.Y. were recipients of Invited Professorships awarded by the University of Tours.

Data availability
No datasets were generated or analysed during the current study.

Declarations

Competing interests
The authors declare no competing interests.

Author details
[1]Université de Tours, Inserm UMR1327 ISCHEMIA, Membrane Signalling and Inflammation in Reperfusion Injuries, 10 Boulevard Tonnellé, Tours 37032, France
[2]Plateforme ASB, Cytometry and Single cell Immunobiology, Université de Tours, CHU Tours, Inserm US61, Tours, France
[3]INRAE, CNRS, Université de Tours, UMR PRC, Nouzilly, France
[4]INRAE, Université de Tours, CHU de Tours, PIXANIM, Nouzilly, France
[5]Henan Medical University, Xinxiang, Henan province, China
[6]School of Biomedical Sciences, University of Leeds, Leeds, UK
[7]Central South University, Changsha, Hunan Province, China
[8]Service de Néphrologie, Dialyse et Transplantation Rénale, CHRU Tours, Tours, France
[9]Fédération Hospitalo-Universitaire Survival Optimization in Organ Transplantation (FHU SUPORT), Tours, France

Received: 22 August 2025 / Accepted: 8 March 2026
Published online: 14 March 2026

References

1. Bray F, Ferlay J, Soerjomataram I, Siegel RL, Torre LA, Jemal A. Global cancer statistics 2018: GLOBOCAN estimates of incidence and mortality worldwide for 36 cancers in 185 countries. CA Cancer J Clin. 2018;68(6):394-424. https://doi.org/10.3322/caac.21492. Epub 2018 Sep 12.
2. Ferro F, Servais S, Besson P, Roger S, Dumas JF, Brisson L. Autophagy and mitophagy in cancer metabolic remodelling. Semin Cell Dev Biol. 2020;98:129–38.
3. Hanahan D, Weinberg RA. Hallmarks of cancer: the next generation. Cell. 2011;144(5):646–74.

4. Becker A, Thakur BK, Weiss JM, Kim HS, Peinado H, Lyden D. Extracellular Vesicles in Cancer: Cell-to-Cell Mediators of Metastasis. Cancer Cell. 2016;30(6):836–48.
5. Ritchie S, Reed DA, Pereira BA, Timpson P. The cancer cell secretome drives cooperative manipulation of the tumour microenvironment to accelerate tumourigenesis. Fac Rev. 2021;10:4.
6. Bebelman MP, Smit MJ, Pegtel DM, Baglio SR. Biogenesis and function of extracellular vesicles in cancer. Pharmacol Ther. 2018;188:1–11.
7. Gatenby RA, Gillies RJ. Why do cancers have high aerobic glycolysis? Nat Rev Cancer. 2004;4(11):891–9.
8. Wang T, Gilkes DM, Takano N, Xiang L, Luo W, Bishop CJ, Chaturvedi P, Green JJ, Semenza GL. Hypoxia-inducible factors and RAB22A mediate formation of microvesicles that stimulate breast cancer invasion and metastasis. Proc Natl Acad Sci U S A. 2014;111(31):E3234–3242.
9. van Niel G, D'Angelo G, Raposo G. Shedding light on the cell biology of extracellular vesicles. Nat Rev Mol Cell Biol. 2018;19(4):213–28.
10. Hessvik NP, Llorente A. Current knowledge on exosome biogenesis and release. Cell Mol Life Sci. 2018;75(2):193–208.
11. Choezom D, Gross JC. Neutral sphingomyelinase 2 controls exosome secretion by counteracting V-ATPase-mediated endosome acidification. J Cell Sci. 2022;135(5):jcs259324. https://doi.org/10.1242/jcs.259324. Epub 2022 Feb 28.
12. van Niel G, Charrin S, Simoes S, Romao M, Rochin L, Saftig P, Marks MS, Rubinstein E, Raposo G. The tetraspanin CD63 regulates ESCRT-independent and -dependent endosomal sorting during melanogenesis. Dev Cell. 2011;21(4):708–21.
13. Huotari J, Helenius A. Endosome maturation. EMBO J. 2011;30(17):3481–500.
14. Ostrowski M, Carmo NB, Krumeich S, Fanget I, Raposo G, Savina A, Moita CF, Schauer K, Hume AN, Freitas RP, et al. Rab27a and Rab27b control different steps of the exosome secretion pathway. Nat Cell Biol. 2010;12(1):19–30. sup pp.
15. Liu C, Liu D, Wang S, Gan L, Yang X, Ma C. Identification of the SNARE complex that mediates the fusion of multivesicular bodies with the plasma membrane in exosome secretion. J Extracell vesicles. 2023;12(9):e12356.
16. Xu J, Camfield R, Gorski SM. The interplay between exosomes and autophagy - partners in crime. J Cell Sci. 2018;131(15):jcs215210. https://doi.org/10.1242/jcs.215210.
17. Jeppesen DK, Fenix AM, Franklin JL, Higginbotham JN, Zhang Q, Zimmerman LJ, Liebler DC, Ping J, Liu Q, Evans R, et al. Reassessment of Exosome Composition. Cell. 2019;177(2):428–45. e418.
18. Wei X, Liang M, Deng M, Zheng J, Luo F, Ma Q. A switch from lysosomal degradation to secretory autophagy initiates osteogenic bone metastasis in prostate cancer. J Extracell vesicles. 2024;13(11):e70002.
19. Xu J, Yang KC, Go NE, Colborne S, Ho CJ, Hosseini-Beheshti E, Lystad AH, Simonsen A, Guns ET, Morin GB, et al. Chloroquine treatment induces secretion of autophagy-related proteins and inclusion of Atg8-family proteins in distinct extracellular vesicle populations. Autophagy. 2022;18(11):2547–60.
20. Bustos SO, Leal Santos N, Chammas R, Andrade LNS. Secretory Autophagy Forges a Therapy Resistant Microenvironment in Melanoma. Cancers. 2022;14(1):234. https://doi.org/10.3390/cancers14010234.
21. Vultaggio-Poma V, Falzoni S, Salvi G, Giuliani AL, Di Virgilio F. Signalling by extracellular nucleotides in health and disease. Biochim Biophys Acta Mol Cell Res. 2022;1869(5):119237.
22. Roger S, Jelassi B, Couillin I, Pelegrin P, Besson P, Jiang LH. Understanding the roles of the P2X7 receptor in solid tumour progression and therapeutic perspectives. Biochim Biophys Acta. 2015;1848(10 Pt B):2584–602.
23. Boccazzi M, Raffaele S, Zanettin T, Abbracchio MP, Fumagalli M. Altered Purinergic Signaling in Neurodevelopmental Disorders: Focus on P2 Receptors. Biomolecules. 2023;13(5):856. https://doi.org/10.3390/biom13050856.
24. Wei L, Syed Mortadza SA, Yan J, Zhang L, Wang L, Yin Y, Li C, Chalon S, Emond P, Belzung C, et al. ATP-activated P2X7 receptor in the pathophysiology of mood disorders and as an emerging target for the development of novel antidepressant therapeutics. Neurosci Biobehav Rev. 2018;87:192–205.
25. Illes P, Muller CE, Jacobson KA, Grutter T, Nicke A, Fountain SJ, Kennedy C, Schmalzing G, Jarvis MF, Stojilkovic SS, et al. Update of P2X receptor properties and their pharmacology: IUPHAR Review 30. Br J Pharmacol. 2021;178(3):489–514.
26. Burnstock G, Fredholm BB, North RA, Verkhratsky A. The birth and postnatal development of purinergic signalling. Acta Physiol (Oxf). 2010;199(2):93–147.
27. Roger S, Gillet L, Baroja-Mazo A, Surprenant A, Pelegrin P. C-terminal calmodulin-binding motif differentially controls human and rat P2X7 receptor current facilitation. J Biol Chem. 2010;285(23):17514–24.
28. Zimmermann H. History of ectonucleotidases and their role in purinergic signaling. Biochem Pharmacol. 2021;187:114322.
29. Duret T, Elmallah M, Rollin J, Gatault P, Jiang LH, Roger S. Role of purinoreceptors in the release of extracellular vesicles and consequences on immune response and cancer progression. Biomed J. 2025;48(3):100805.
30. Jiang LH, Roger S. Heterologous Expression and Patch-Clamp Recording of P2X Receptors in HEK293 Cells. Methods Mol Biol. 2020;2041:261–73.
31. Di Virgilio F, Vultaggio-Poma V, Sarti AC. P2X receptors in cancer growth and progression. Biochem Pharmacol. 2021;187:114350.
32. Di Virgilio F, Ferrari D, Adinolfi E. P2X(7): a growth-promoting receptor-implications for cancer. Purinergic Signal. 2009;5(2):251–6.
33. Jelassi B, Anchelin M, Chamouton J, Cayuela ML, Clarysse L, Li J, Gore J, Jiang LH, Roger S. Anthraquinone emodin inhibits human cancer cell invasiveness by antagonizing P2X7 receptors. Carcinogenesis. 2013;34(7):1487–96.
34. Jelassi B, Chantome A, Alcaraz-Perez F, Baroja-Mazo A, Cayuela ML, Pelegrin P, Surprenant A, Roger S. P2X(7) receptor activation enhances SK3 channels-and cystein cathepsin-dependent cancer cells invasiveness. Oncogene. 2011;30(18):2108–22.
35. Brisson L, Chadet S, Lopez-Charcas O, Jelassi B, Ternant D, Chamouton J, Lerondel S, Le Pape A, Couillin I, Gombault A et al. P2X7 Receptor Promotes Mouse Mammary Cancer Cell Invasiveness and Tumour Progression, and Is a Target for Anticancer Treatment. Cancers. 2020;12(9):2342. https://doi.org/10.3390/cancers12092342.
36. Adinolfi E, De Marchi E, Orioli E, Pegoraro A, Di Virgilio F. Role of the P2X7 receptor in tumor-associated inflammation. Curr Opin Pharmacol. 2019;47:59–64.
37. Yang Y, Wang H, Kouadir M, Song H, Shi F. Recent advances in the mechanisms of NLRP3 inflammasome activation and its inhibitors. Cell Death Dis. 2019;10(2):128.
38. MacKenzie A, Wilson HL, Kiss-Toth E, Dower SK, North RA, Surprenant A. Rapid secretion of interleukin-1beta by microvesicle shedding. Immunity. 2001;15(5):825–35.
39. Qu Y, Franchi L, Nunez G, Dubyak GR. Nonclassical IL-1 beta secretion stimulated by P2X7 receptors is dependent on inflammasome activation and correlated with exosome release in murine macrophages. J Immunol. 2007;179(3):1913–25.
40. Pizzirani C, Ferrari D, Chiozzi P, Adinolfi E, Sandona D, Savaglio E, Di Virgilio F. Stimulation of P2 receptors causes release of IL-1beta-loaded microvesicles from human dendritic cells. Blood. 2007;109(9):3856–64.
41. Pegoraro A, De Marchi E, Ferracin M, Orioli E, Zanoni M, Bassi C, Tesei A, Capece M, Dika E, Negrini M, et al. P2X7 promotes metastatic spreading and triggers release of miRNA-containing exosomes and microvesicles from melanoma cells. Cell Death Dis. 2021;12(12):1088.
42. Murrell-Lagnado RD, Frick M. P2X4 and lysosome fusion. Curr Opin Pharmacol. 2019;47:126–32.
43. He J, Zhou Y, Arredondo Carrera HM, Sprules A, Neagu R, Zarkesh SA, Eaton C, Luo J, Gartland A, Wang N. Inhibiting the P2X4 Receptor Suppresses Prostate Cancer Growth In Vitro and In Vivo, Suggesting a Potential Clinical Target. Cells. 2020;9(11):2511. https://doi.org/10.3390/cells9112511.
44. Maynard JP, Lu J, Vidal I, Hicks J, Mummert L, Ali T, Kempski R, Carter AM, Sosa RY, Peiffer LB, et al. P2X4 purinergic receptors offer a therapeutic target for aggressive prostate cancer. J Pathol. 2022;256(2):149–63.
45. Chadet S, Allard J, Brisson L, Lopez-Charcas O, Lemoine R, Heraud A, Lerondel S, Guibon R, Fromont G, Le Pape A, et al. P2x4 receptor promotes mammary cancer progression by sustaining autophagy and associated mesenchymal transition. Oncogene. 2022;41(21):2920–31.
46. Kim OK, Nam DE, Hahn YS. The Pannexin 1/Purinergic Receptor P2X4 Pathway Controls the Secretion of MicroRNA-Containing Exosomes by HCV-Infected Hepatocytes. Hepatology. 2021;74(6):3409–26.
47. Consortium E-T, Van Deun J, Mestdagh P, Agostinis P, Akay O, Anand S, Anckaert J, Martinez ZA, Baetens T, Beghein E, et al. EV-TRACK: transparent reporting and centralizing knowledge in extracellular vesicle research. Nat Methods. 2017;14(3):228–32.
48. Fonseka P, Pathan M, Chitti SV, Kang T, Mathivanan S. FunRich enables enrichment analysis of OMICs datasets. J Mol Biol. 2021;433(11):166747.
49. Chitti SV, Gummadi S, Kang T, Shahi S, Marzan AL, Nedeva C, Sanwlani R, Bramich K, Stewart S, Petrovska M, et al. Vesiclepedia 2024: an extracellular vesicles and extracellular particles repository. Nucleic Acids Res. 2024;52(D1):D1694–8.
50. Pols MS, Klumperman J. Trafficking and function of the tetraspanin CD63. Exp Cell Res. 2009;315(9):1584–92.

51. Chen G, Huang AC, Zhang W, Zhang G, Wu M, Xu W, Yu Z, Yang J, Wang B, Sun H, et al. Exosomal PD-L1 contributes to immunosuppression and is associated with anti-PD-1 response. Nature. 2018;560(7718):382–6.
52. Nielsen E, Severin F, Backer JM, Hyman AA, Zerial M. Rab5 regulates motility of early endosomes on microtubules. Nat Cell Biol. 1999;1(6):376–82.
53. Hsu C, Morohashi Y, Yoshimura S, Manrique-Hoyos N, Jung S, Lauterbach MA, Bakhti M, Gronborg M, Mobius W, Rhee J, et al. Regulation of exosome secretion by Rab35 and its GTPase-activating proteins TBC1D10A-C. J Cell Biol. 2010;189(2):223–32.
54. Gutierrez MG, Munafo DB, Beron W, Colombo MI. Rab7 is required for the normal progression of the autophagic pathway in mammalian cells. J Cell Sci. 2004;117(Pt 13):2687–97.
55. Sun C, Wang P, Dong W, Liu H, Sun J, Zhao L. LncRNA PVT1 promotes exosome secretion through YKT6, RAB7, and VAMP3 in pancreatic cancer. Aging. 2020;12(11):10427–40.
56. Friand V, David G, Zimmermann P. Syntenin and syndecan in the biogenesis of exosomes. Biol Cell. 2015;107(10):331–41.
57. Roger S, Pelegrin P. P2X7 receptor antagonism in the treatment of cancers. Expert Opin Investig Drugs. 2011;20(7):875–80.
58. Janho Dit Hreich S, Benzaquen J, Hofman P, Vouret-Craviari V. To inhibit or to boost the ATP/P2RX7 pathway to fight cancer-that is the question. Purinergic Signal. 2021;17(4):619–31.
59. Adinolfi E, Capece M, Franceschini A, Falzoni S, Giuliani AL, Rotondo A, Sarti AC, Bonora M, Syberg S, Corigliano D, et al. Accelerated tumor progression in mice lacking the ATP receptor P2X7. Cancer Res. 2015;75(4):635–44.
60. Ghiringhelli F, Apetoh L, Tesniere A, Aymeric L, Ma Y, Ortiz C, Vermaelen K, Panaretakis T, Mignot G, Ullrich E, et al. Activation of the NLRP3 inflammasome in dendritic cells induces IL-1beta-dependent adaptive immunity against tumors. Nat Med. 2009;15(10):1170–8.
61. Qu Y, Ramachandra L, Mohr S, Franchi L, Harding CV, Nunez G, Dubyak GR. P2X7 receptor-stimulated secretion of MHC class II-containing exosomes requires the ASC/NLRP3 inflammasome but is independent of caspase-1. J Immunol. 2009;182(8):5052–62.
62. Zhang J, Yu Z, Wang M, Kang X, Wu X, Yang F, Yang L, Sun S, Wu LA. Enhanced exosome secretion regulated by microglial P2X7R in the medullary dorsal horn contributes to pulpitis-induced pain. Cell Biosci. 2025;15(1):28.
63. Carotti V, Rigalli JP, van Asbeck-van der Wijst J, Hoenderop JGJ. Interplay between purinergic signalling and extracellular vesicles in health and disease. Biochem Pharmacol. 2022;203:115192.
64. Park M, Kim J, Phuong NTT, Park JG, Park JH, Kim YC, Baek MC, Lim SC, Kang KW. Involvement of the P2X7 receptor in the migration and metastasis of tamoxifen-resistant breast cancer: effects on small extracellular vesicles production. Sci Rep. 2019;9(1):11587.
65. O'Brien K, Rani S, Corcoran C, Wallace R, Hughes L, Friel AM, McDonnell S, Crown J, Radomski MW, O'Driscoll L. Exosomes from triple-negative breast cancer cells can transfer phenotypic traits representing their cells of origin to secondary cells. Eur J Cancer. 2013;49(8):1845–59.
66. Nigri J, Leca J, Tubiana SS, Finetti P, Guillaumond F, Martinez S, Lac S, Iovanna JL, Audebert S, Camoin L, et al. CD9 mediates the uptake of extracellular vesicles from cancer-associated fibroblasts that promote pancreatic cancer cell aggressiveness. Sci Signal. 2022;15(745):eabg8191.
67. Zhang Z, Chen G, Zhou W, Song A, Xu T, Luo Q, Wang W, Gu XS, Duan S. Regulated ATP release from astrocytes through lysosome exocytosis. Nat Cell Biol. 2007;9(8):945–53.
68. Huang P, Zou Y, Zhong XZ, Cao Q, Zhao K, Zhu MX, Murrell-Lagnado R, Dong XP. P2X4 Forms Functional ATP-activated Cation Channels on Lysosomal Membranes Regulated by Luminal pH. J Biol Chem. 2014;289(25):17658–67.
69. Xu H, Ren D. Lysosomal physiology. Annu Rev Physiol. 2015;77:57–80.
70. Ganesan D, Cai Q. Understanding amphisomes. Biochem J. 2021;478(10):1959–76.
71. Lauritzen I, Bini A, Becot A, Gay AS, Badot C, Pagnotta S, Chami M, Checler F. Presenilins as hub proteins controlling the endocytic and autophagic pathways and small extracellular vesicle secretion. J Extracell vesicles. 2025;14(1):e70019.
72. Ortega FG, Roefs MT, de Miguel Perez D, Kooijmans SA, de Jong OG, Sluijter JP, Schiffelers RM, Vader P. Interfering with endolysosomal trafficking enhances release of bioactive exosomes. Nanomedicine. 2019;20:102014.
73. Bucci C, Thomsen P, Nicoziani P, McCarthy J, van Deurs B. Rab7: a key to lysosome biogenesis. Mol Biol Cell. 2000;11(2):467–80.
74. Baietti MF, Zhang Z, Mortier E, Melchior A, Degeest G, Geeraerts A, Ivarsson Y, Depoortere F, Coomans C, Vermeiren E, et al. Syndecan-syntenin-ALIX regulates the biogenesis of exosomes. Nat Cell Biol. 2012;14(7):677–85.
75. Vodicka P, Lim J, Williams DT, Kegel KB, Chase K, Park H, Marchionini D, Wilkinson S, Mead T, Birch H, et al. Assessment of chloroquine treatment for modulating autophagy flux in brain of WT and HD mice. J Huntingtons Dis. 2014;3(2):159–74.

Publisher's Note